



**HAL**  
open science

**Fe<sub>2.5</sub>Co<sub>0.3</sub>Zn<sub>0.2</sub>O<sub>4</sub>/CuCr-LDH as a  
visible-light-responsive photocatalyst for the  
degradation of caffeine, bisphenol A, and simazine in  
pure water and real wastewater under photo-Fenton-like  
degradation process**

Arezou Fazli, Marcello Brigante, Alireza Khataee, Gilles Mailhot

► **To cite this version:**

Arezou Fazli, Marcello Brigante, Alireza Khataee, Gilles Mailhot. Fe<sub>2.5</sub>Co<sub>0.3</sub>Zn<sub>0.2</sub>O<sub>4</sub>/CuCr-LDH as a visible-light-responsive photocatalyst for the degradation of caffeine, bisphenol A, and simazine in pure water and real wastewater under photo-Fenton-like degradation process. *Chemosphere*, 2022, 291, pp.132920. 10.1016/j.chemosphere.2021.132920 . hal-03634868

**HAL Id: hal-03634868**

**<https://hal.science/hal-03634868v1>**

Submitted on 28 Nov 2022

**HAL** is a multi-disciplinary open access archive for the deposit and dissemination of scientific research documents, whether they are published or not. The documents may come from teaching and research institutions in France or abroad, or from public or private research centers.

L'archive ouverte pluridisciplinaire **HAL**, est destinée au dépôt et à la diffusion de documents scientifiques de niveau recherche, publiés ou non, émanant des établissements d'enseignement et de recherche français ou étrangers, des laboratoires publics ou privés.



Distributed under a Creative Commons Attribution - NonCommercial - NoDerivatives 4.0  
International License

1 **Fe<sub>2.5</sub>Co<sub>0.3</sub>Zn<sub>0.2</sub>O<sub>4</sub>/CuCr-LDH as a visible-light-responsive photocatalyst for**  
2 **the degradation of Caffeine, Bisphenol A, and Simazine in pure water and**  
3 **real wastewater under photo-Fenton-like degradation process**

4  
5 **Arezou Fazli<sup>a, b</sup>, Marcello Brigante<sup>a</sup>, Alireza Khataee<sup>b, c\*</sup>, Gilles Mailhot<sup>a\*</sup>**

6 *<sup>a</sup> Université Clermont Auvergne, CNRS, SIGMA Clermont, Institut de Chimie de Clermont-*  
7 *Ferrand, F-63000 Clermont-Ferrand, France*

8 *<sup>b</sup> Research Laboratory of Advanced Water and Wastewater Treatment Processes, Department*  
9 *of Applied Chemistry, Faculty of Chemistry, University of Tabriz, 51666-16471, Tabriz, Iran*

10 *<sup>c</sup> Department of Environmental Engineering, Gebze Technical University, 41400 Gebze, Turkey*

11  
12  
13  
14  
15  
16  
17  
18  
19  
20  
21  
22  
23  
24  
25 \* Corresponding authors:

26 a\_khataee@tabrizu.ac.ir (A. Khataee)  
27 gilles.mailhot@uca.fr (G. Mailhot)

28 **Abstract**

29 This paper outlines the synthesis and application of a sustainable composite for the photo-  
30 Fenton-like degradation of caffeine, bisphenol A, and simazine. The phase, morphology, optical  
31 and magnetic properties of the samples were evaluated by different characterization techniques.  
32 The composite of  $\text{Fe}_{2.5}\text{Co}_{0.3}\text{Zn}_{0.2}\text{O}_4$  and copper-chromium layered double hydroxide (CuCr-  
33 LDH) was determined to be the most favorable photocatalyst in the photo-Fenton-like process  
34 when compared with  $\text{Fe}_3\text{O}_4$ ,  $\text{Fe}_{2.5}\text{Co}_{0.3}\text{Zn}_{0.2}\text{O}_4$ , CuCr-LDH, and  $\text{Fe}_3\text{O}_4/\text{CuCr-LDH}$  composite.  
35 Studying the efficiency of the photo-Fenton-like degradation process in the presence of the  
36  $\text{Fe}_{2.5}\text{Co}_{0.3}\text{Zn}_{0.2}\text{O}_4/\text{CuCr-LDH}$  composite revealed a degradation rate constant of caffeine twice  
37 more than the sum of those obtained for the individual processes. This ascribes to the synergistic  
38 effect by which the photo-generated electron-hole from the catalyst and the efficient reduction  
39 of  $\text{Fe}^{3+}$ ,  $\text{Cu}^{2+}$ , etc. during the photo-Fenton-like reaction is accelerated. Moreover, under the  
40 optimal condition and after 120 min of heterogenous photo-Fenton-like process at natural pH,  
41 > 90% of pollutants mixture was decomposed. The experiments fulfilled in near-real conditions  
42 demonstrated I) the high stability and magnetically recoverability of the photocatalyst and II)  
43 the proper degradation performance of the applied heterogenous photo-Fenton-process in the  
44 removal of pollutant mixture in different water bodies and in the presence of chloride and  
45 bicarbonate ions.

46

47 **Keywords:** Sustainable photocatalyst; CuCr-LDH; Doped magnetite; Mineralization;  
48 Micropollutants mixture.

49

50

## 51 **1. Introduction**

52 Industrial toxic wastes like pharmaceuticals, pesticides, and phenols are present in water and  
53 wastewater, which turned into a globally concerning issue. Caffeine (CAF) is a widely used  
54 psychoactive medicine and it can be found in coffee seeds (0.43 to 0.82 mg/mL), tea leaves,  
55 etc. (Chen et al., 2018). Some industrial raw materials such as bisphenol A (BPA) are being  
56 used for the preparation of water bottles, food containers, and polycarbonates. Nevertheless,  
57 according to the World Health Organization (WHO), a low concentration of BPA can result in  
58 hypertension and cell disorders (Chen et al., 2020). Furthermore, different s-triazine herbicides  
59 have been used in the agriculture to manage the broadleaf and grassy weeds (X. Yang et al.,  
60 2020). Due to the excessive usage of the herbicides such as simazine (SIM), a different amount  
61 of them has appeared in groundwater which leads to DNA replication and disorders in the  
62 central nervous system (Nahim-Granados et al., 2020). Due to the entrance of the above-  
63 mentioned compounds to the water bodies, researchers have recently focused on the  
64 performance of various treatment processes for the degradation of an individual kind of  
65 pollutant (Hieu et al., 2021). However, it is well-known that real wastewater comprises a  
66 mixture of diverse kinds of pollutants which should be treated before their arrival into aquatic  
67 ecosystems (Chavan and Fulekar, 2020).

68 As the representative AOPs, the Fenton processes can activate  $\text{H}_2\text{O}_2$  (HP) by the Fenton  
69 reagent  $\text{Fe}^{2+}$  to produce reactive  $\cdot\text{OH}$  (Brillas, 2020). So far, different inherent shortcomings  
70 such as higher efficiencies at acidic pHs and the rapid decay of the utilized catalyst confined  
71 their usage for practical applications (Zhang et al., 2020). To overcome these restrictions, the  
72 photo-Fenton processes in the presence of a photocatalyst is of great consideration. The photo-  
73 generated electron and hole pairs in the photocatalysts promote the regeneration of Fenton  
74 reagent  $\text{Fe}^{2+}$  which is favourable for the Fenton reactions (Sharma et al., 2020). In this context,  
75 a big effort has been devoted to design the effective heterogeneous photocatalysts grounded on

76 the advantages such as high activity in different pH values and efficient recovery from the  
77 reaction media (Sharma et al., 2020). Layered double hydroxides (LDHs) are a class of two-  
78 dimensional (2D) synthetic compounds with a high specific structure and chemical stability  
79 which make them suitable candidates for the varied catalytic degradation processes (Wu et al.,  
80 2022). For instance, Bai et al. (Bai et al., 2017) and Li et al. (Li et al., 2020) used Co-Fe-LDH  
81 and Zn-Al-LDH as Fenton and photo-Fenton catalysts to degraded different water pollutants,  
82 respectively. Besides the higher photocatalytic activity, recoverability and reusability of the  
83 nanoscale photocatalysts after degradation reactions are of great consideration for sustainable  
84 process management (Fazli et al., 2021b). In order to recover LDHs from the reaction media by  
85 a permanent magnet, different LDH heterojunctions with magnetic materials have been  
86 synthesized and used in AOPs (Gonçalves et al., 2019).

87 In previous work, the activation of persulfate and HP in the presence of  $\text{Fe}_{2.5}\text{Co}_{0.3}\text{Zn}_{0.2}\text{O}_4$   
88 nanoparticles to decompose a pharmaceutical water pollutant was studied. It was found out that  
89 the nanoparticles were magnetically separable; however, under UVA illumination and the  
90 solution pH of 8, the co-doped magnetite had lower efficiency for the activation of HP (Fazli et  
91 al., 2021b). Therefore, it would be of great importance to add a highly active semiconductor to  
92 co-doped magnetite to prepare a high-performance and environmentally friendly photocatalyst  
93 for the photo-Fenton-like process. Considering the reaction rate constant of Fe (III) ( $10^{-3}$ – $10^{-2}$   
94  $\text{M}^{-1} \text{s}^{-1}$ ), Fe (II) ( $76 \text{M}^{-1} \text{s}^{-1}$ ), Cu (I) ( $10^4 \text{M}^{-1} \text{s}^{-1}$ ) and Cu (II) ( $4.6 \times 10^2 \text{M}^{-1} \text{s}^{-1}$ ), copper can  
95 react with HP faster (Xiao et al., 2020). Moreover, previous works have confirmed the high  
96 impact of chromium on the further production of hydroxyl radicals in the UV/Fenton system  
97 (Liang et al., 2012). Therefore, herein, we synthesized a CuCr-LDH as the proper  
98 semiconductor and merged its merits with the magnetically separable  $\text{Fe}_{2.5}\text{Co}_{0.3}\text{Zn}_{0.2}\text{O}_4$   
99 nanoparticles to prepare an efficient visible-light-responsive photocatalyst for the photo-  
100 Fenton-like degradation of 3 kinds of water contaminants. To the authors' knowledge, no

101 research was devoted to studying the effect of  $\text{Fe}_{2.5}\text{Co}_{0.3}\text{Zn}_{0.2}\text{O}_4/\text{CuCr-LDH}$  composite in the  
102 photo-Fenton-like degradation of pollutant mixture in pure water and real wastewater.  
103 Therefore, the proposed research study was undertaken with the following goals: a) to prepare  
104 a visible-light responsive magnetic composite ( $\text{Fe}_{2.5}\text{Co}_{0.3}\text{Zn}_{0.2}\text{O}_4/\text{CuCr-LDH}$ ); (b) investigate  
105 the optical, magnetic, and physicochemical properties of the composite, (c) study the  
106 performance of the so-synthesized photocatalysts for the photo-Fenton-like degradation of  
107 water pollutants, (d) examine the stability and reusability of so-synthesized photocatalyst, (e)  
108 investigate the effect of inorganic anions and radical scavengers, (f) assess the performance of  
109 composite as the photo-Fenton-like photocatalyst for the effective degradation of pollutants  
110 mixture in pure and tap water, as well as real wastewater matrix, and finally (g) examine the  
111 efficiency of the photo-Fenton-like process for the mineralization of the pollutants mixture.

112

## 113 **2. Experimental**

### 114 **2.1. Materials**

115  $\text{CoCl}_2 \cdot 6\text{H}_2\text{O}$  97%,  $\text{NaNO}_3$  99%,  $\text{FeCl}_2 \cdot 4\text{H}_2\text{O}$  99%,  $\text{ZnCl}_2 \cdot 4\text{H}_2\text{O}$  98%,  $\text{HCl}$  38%,  $\text{N}_2\text{H}_4 \cdot \text{H}_2\text{O}$   
116 90–100%,  $\text{NaOH}$  99%,  $\text{Cu}(\text{NO}_3)_2 \cdot 3\text{H}_2\text{O}$  99%,  $\text{Cr}(\text{NO}_3)_3 \cdot 9\text{H}_2\text{O}$  99%,  $\text{H}_2\text{O}_2$  30%,  $\text{KI}$  99.5%,  
117  $\text{NaHCO}_3$ , 99.7%,  $\text{NaCl}$ , 99% and organic solvents (purity greater than 99%) were provided  
118 from Sigma Aldrich France and used with no further purification.

119

### 120 **2.2. Preparation of the photocatalysts**

121 The required solutions were prepared with previously deoxygenated distilled water via argon  
122 gas. The typical procedure to synthesize the  $\text{Fe}_{2.5}\text{Co}_{0.3}\text{Zn}_{0.2}\text{O}_4/\text{CuCr-LDH}$  composite is  
123 summarized in Fig. S1. As the first step, we synthesized Co and Zn co-doped  $\text{Fe}_3\text{O}_4$   
124 nanoparticles by applying the method explained in our previous work (Fazli et al., 2021c). In  
125 this regard, a 100 mL solution comprised of  $\text{FeCl}_2$ ,  $\text{H}_2\text{O}$ ,  $\text{ZnCl}_2 \cdot 4\text{H}_2\text{O}$ , and  $\text{CoCl}_2 \cdot 6\text{H}_2\text{O}$  and

126 10 mL of HCl (0.6 M) was prepared and added to the three-neck flask. The solution was stirred  
127 at 500 rpm, and then 1 mL hydrazine was added to the solution to reach lower solution pH.  
128 Afterward, the alkaline solution comprised of NaNO<sub>3</sub> (0.9 M) and NaOH (0.4 M), was added  
129 drop by drop to the solution. After the addition of the alkaline solution with the speed of 3  
130 drops/second, the mixture was stirred for 2 h at 95 °C. The resulted particles were magnetically  
131 collected, washed three times with distilled water, and finally dried at 90 °C for 24 h.

132 In the following, the obtained nanoparticles were used to prepare the  
133 Fe<sub>2.5</sub>Co<sub>0.3</sub>Zn<sub>0.2</sub>O<sub>4</sub>/CuCr-LDH composite. For this purpose, two separated solutions (I and II)  
134 were prepared as follows: Solution I: 0.5 g of the so-synthesized co-doped magnetite was  
135 dispersed in 150 mL of water for 30 min; after that, 150 mL of NaOH (2 M) was added drop  
136 by drop. At the same time, the specific amount of Cr (NO<sub>3</sub>)<sub>3</sub>·9H<sub>2</sub>O (0.25 M) and Cu  
137 (NO<sub>3</sub>)<sub>2</sub>·3H<sub>2</sub>O (0.5 M) were respectively dissolved in 50 and 100 mL of distilled water and  
138 mixed with each other to prepare a solution of 150 mL as the salts solution (II). Thereafter,  
139 solutions I and II were mixed drop by drop; while, the mixture was vigorously stirring and the  
140 pH was being kept between 9.3 and 10. The final mixture was aged for 24 h. As the final step,  
141 the particles of the composite were magnetically separated, rinsed three times with water, and  
142 dried at 60 °C for 12 h. Pure CuCr-LDH was prepared with the same procedure without adding  
143 co-doped Fe<sub>3</sub>O<sub>4</sub>.

### 144 **2.3. Characterization**

145 X-ray diffraction (XRD, D8 Advance, Bruker, Germany) and X-ray photoelectron  
146 spectroscopy (XPS, OMICRON EA125, Germany) were utilized to investigate the structural  
147 properties of the samples. SEM (Tescan Mira3, Czech Republic, equipped with a Zeiss Sigma  
148 300) and TEM (H-7650, AMT40, Germany) were used to studying the surface morphology of  
149 the samples. Also, a 3 Flex instrument (Micromeritics, USA) was used to determine the surface  
150 area of the prepared nanomaterials based on the adsorption-desorption isotherms. UV–visible

151 diffuse reflectance spectrophotometry (UV-Vis DRS, S 250, Germany) and a vibrating sample  
152 magnetometer (VSM, Lakeshore, 7400 Series) were used to study the optical and magnetic  
153 aspects of the prepared nanoparticles.

154

#### 155 **2.4. Photo-Fenton-like catalytic tests**

156 According to the picture inserted in Fig. S1, all the experiments were carried out in a 50 mL  
157 Pyrex cylindrical photocatalytic reactor. Meanwhile, a solar simulator lamp (Ocean optics)  
158 fitted with cut-off filters at  $\lambda \geq 400$  nm was used to simulate the vis-light. Fig. S2 shows the  
159 emission spectra related to the abovementioned lamp with and without using a filter. The light  
160 source was placed at a 15 cm distance from the reactor. In order to control the temperature, a  
161 water circulator system was embedded around the reactor. For each run, 50 mL of pollutants  
162 solution with the concentration of 50  $\mu\text{M}$  was prepared and after adding a certain amount of  
163 catalyst the pH of the solution was adjusted to be 8. Prior to irradiation, the minimum time  
164 needed for the maximum adsorption of organic pollutants on the surface of the catalyst was  
165 studied by stirring the suspension in dark. It was found out that the maximum adsorption of  
166 three target pollutants was reached approximately after 30 min of stirring. Therefore, after 30  
167 min of stirring in dark, the predetermined amount of HP was added to the suspension and the  
168 irradiation of the suspension was started. Several samples were collected after 15 min, filtered,  
169 and passed to a vial with 20  $\mu\text{L}$  of methanol to stop the possible reactions. A high-performance  
170 liquid chromatography (Alliance, waters, USA) using a C18 column was applied for measuring  
171 the concentration of remaining pollutants in the reaction media. UPLC condition: injection  
172 volume of 10  $\mu\text{L}$ , flow rate of 0.2  $\text{mL min}^{-1}$ , and isocratic elution comprising of 40 %  
173 acetonitrile and 60 % ultrapure water were used as the best method for the detection of  
174 pollutants. The retention time for CAF, BPA, and SIM was found to be 1.4, 4.4, and 3 min,  
175 respectively. The relative pollutant concentration (%) in the reaction was determined from the



176 decay of pollutants as  $\frac{C_t}{C_0}$  during the reaction time where  $C_0$  and  $C_t$  are the initial concentration  
177 and remaining concentration at time  $t$ , respectively. The reusability of the composite was studied  
178 by collecting it after each degradation run and reusing it for other runs. Moreover, a TOC  
179 analyzer (Shimadzu, TOC-L, Japan) was used for monitoring the mineralization of pollutants.  
180 The dissolved concentrations of Cu, Cr, Fe, Co, and Zn were measured by an inductively  
181 coupled plasma emission spectroscopy (ICP-AES, Jobin-Yvon ULTIMA C, USA). The real  
182 wastewater was obtained at the outlet of the treatment from the “3 rivières” urban STP,  
183 Clermont-Ferrand, France in December 2019 and main physico-chemical parameters are  
184 reported elsewhere (Fazli et al., 2021c).

185

### 186 **3. Results and discussion**

#### 187 **3.1. Characterization**

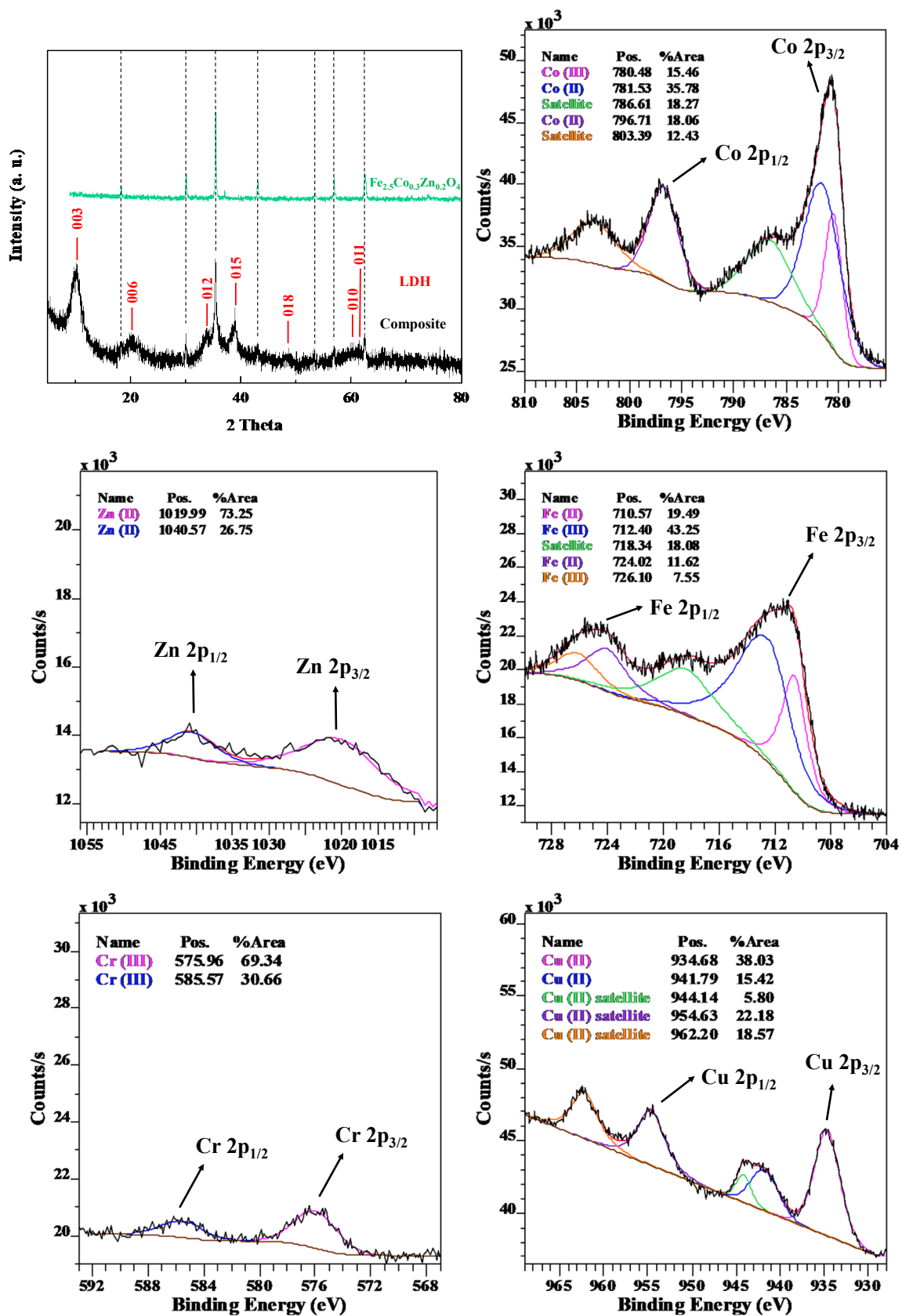
##### 188 **3.1.1. Phase analysis: XRD and XPS**

189 The XRD patterns of the so-synthesized samples were plotted together for comparison in  
190 Fig. 1. From the results, it is evident that the obtained positions of peaks for co-doped magnetite  
191 are consistent with the standard diffraction data for magnetite (JCPDS file no. 01–089-0951)  
192 (Fazli et al., 2021c). Furthermore, the XRD pattern related to the  $\text{Fe}_{2.5}\text{Co}_{0.3}\text{Zn}_{0.2}\text{O}_4/\text{CuCr-LDH}$   
193 composite proved the existence of the specific peaks at the  $2\theta$  values of  $18^\circ$ ,  $30.05^\circ$ ,  $35.9^\circ$ ,  
194  $36.7^\circ$ ,  $43.6^\circ$ ,  $54.1^\circ$ ,  $57.5^\circ$ , and  $62.5^\circ$  relating to the co-doped magnetite and also the peaks at  
195  $10.66^\circ$ ,  $21^\circ$ ,  $35.1^\circ$ ,  $38^\circ$ ,  $47.05^\circ$ ,  $60.05^\circ$ , and  $61.5^\circ$  corresponding to CuCr-LDH (JCPDS file no.  
196 00-035-0965) (Aghaziarati et al., 2020). The co-existence of the related peaks proved that the  
197 phase of co-doped magnetite and LDH are well coupled with each other. In addition, no more  
198 irrelevant peaks were observed in the XRD pattern of the composite, which revealed the purity  
199 and crystallinity of the sample. However, in comparison with pure  $\text{Fe}_{2.5}\text{Co}_{0.3}\text{Zn}_{0.2}\text{O}_4$

200 nanoparticles and LDH, the intensity of the related peaks in the XRD pattern of the composite  
201 was mitigated. This phenomenon has been widely related to the weak crystallinity nature of the  
202 composite arising from the formation of heterojunction between  $\text{Fe}_{2.5}\text{Co}_{0.3}\text{Zn}_{0.2}\text{O}_4$  and co-doped  
203 magnetite.

204 Furthermore, the high-resolution XPS (HRXPS) spectra of the so-synthesized  
205 nanocomposite have been presented in Fig. 1. Considering the observed sub-peaks, the binding  
206 energies of 710.57 and 724.02 eV ascertain the existence of Fe (II), while the related peaks for  
207 Fe (III) are located in the 712.40 and 726.10 eV (Fazli et al., 2021c). The observed satellite  
208 (shoulder) peaks are in coherence with the reported results of the other researchers (Rad et al.,  
209 2018; Yamashita and Hayes, 2008) and affirm the presence of Fe (II). Moreover, the spectrum  
210 corresponding to Co  $2p_{1/2}$ , Co  $2p_{3/2}$  revealed the presence of Co (II) (781.53 eV and 796.71 eV)  
211 and Co (III) (780.6 eV) on the surface of the composite (Chen et al., 2014). The existence of  
212 Zn  $2p_{3/2}$  and Zn  $2p_{1/2}$  were affirmed with the binding energies at 1019.99 eV and 1040.57 eV  
213 (Nguyen et al., 2021), respectively. Furthermore, considering the HRXPS peak related to Cu  
214  $2p$ , the signals of Cu (II) was observed at 954.63 eV (Liu et al., 2016; Wu et al., 2006). An other  
215 peak at 934.68 eV also confirmed the presence of Cu (II) (Liu et al., 2016; Wu et al., 2006). It  
216 is worth noting that the satellite peaks characterize the materials which possess a  $d^9$   
217 configuration in the ground state (Wu et al., 2006). Concerning this fact, the appeared peaks at  
218 941.79 eV, 944.14 eV, and 962.20 eV relate to the  $3d^9$  shell of Cu (II) (Liu et al., 2016). Finally,  
219 Cr (III) has been recognized by the peaks positioned at the emerged peaks at 575.96 eV and  
220 585.57 eV for Cr  $2p$ .

221



222

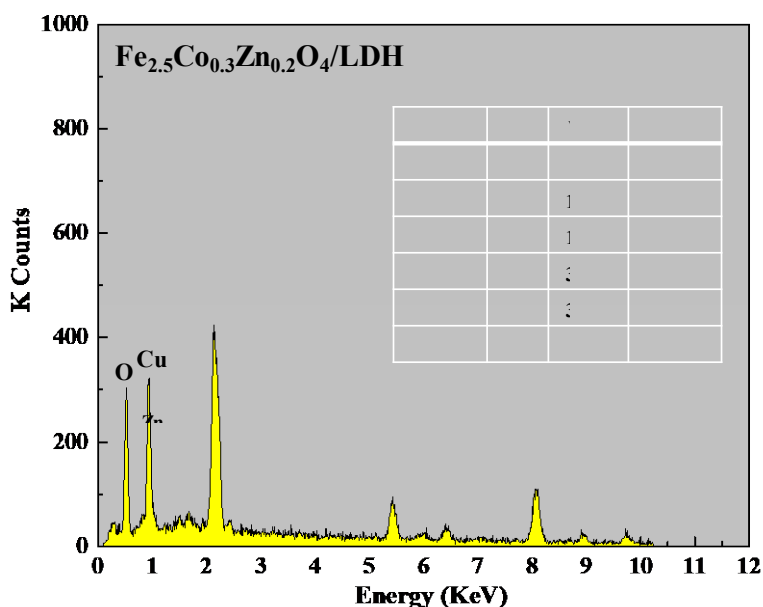
223 Fig. 1. XRD 2θ scans for the so-synthesized photocatalysts and high-resolution XPS spectra

224 of Fe 2p, Zn 2p, Co 2p, Cu 2p, and Cr 2P of Fe<sub>2.5</sub>Co<sub>0.3</sub>Zn<sub>0.2</sub>O<sub>4</sub>/CuCr-LDH composite.

225 **3.1.2. Morphological analysis**

226 Fig. S3 (a-c) shows the SEM images of  $\text{Fe}_{2.5}\text{Co}_{0.3}\text{Zn}_{0.2}\text{O}_4$ , CuCr-LDH, and  
227  $\text{Fe}_{2.5}\text{Co}_{0.3}\text{Zn}_{0.2}\text{O}_4/\text{CuCr-LDH}$  composite. The cubic and lamellar structures were observed for  
228 the co-doped magnetite and pure LDH, whereas, the SEM image corresponding to the  
229 composite revealed the coverage of co-doped magnetite nanoparticles with the LDH layers.  
230 This was further proved by the TEM images (Fig. S3 (d-e)) and SEM elemental mapping.  
231 According to the magnified TEM image of the composite, the composite consists of the cubic  
232 co-doped magnetite and layers of Cu-Cr-LDH. Notably, Fig. 2 depicts the EDX spectra with  
233 the relative weight and atomic percentage of the elements.

234



235

236 **Fig. 2.** The EDX spectrum of the  $\text{Fe}_{2.5}\text{Co}_{0.3}\text{Zn}_{0.2}\text{O}_4/\text{CuCr-LDH}$  composite.

237

238 Moreover, based on Fig. 3 which present the SEM elemental mapping it can be deduced that  
239 the composite contains the elements such as Co, Cr, Cu, Zn, and Fe which have been uniformly  
240 distributed on the surface.

241

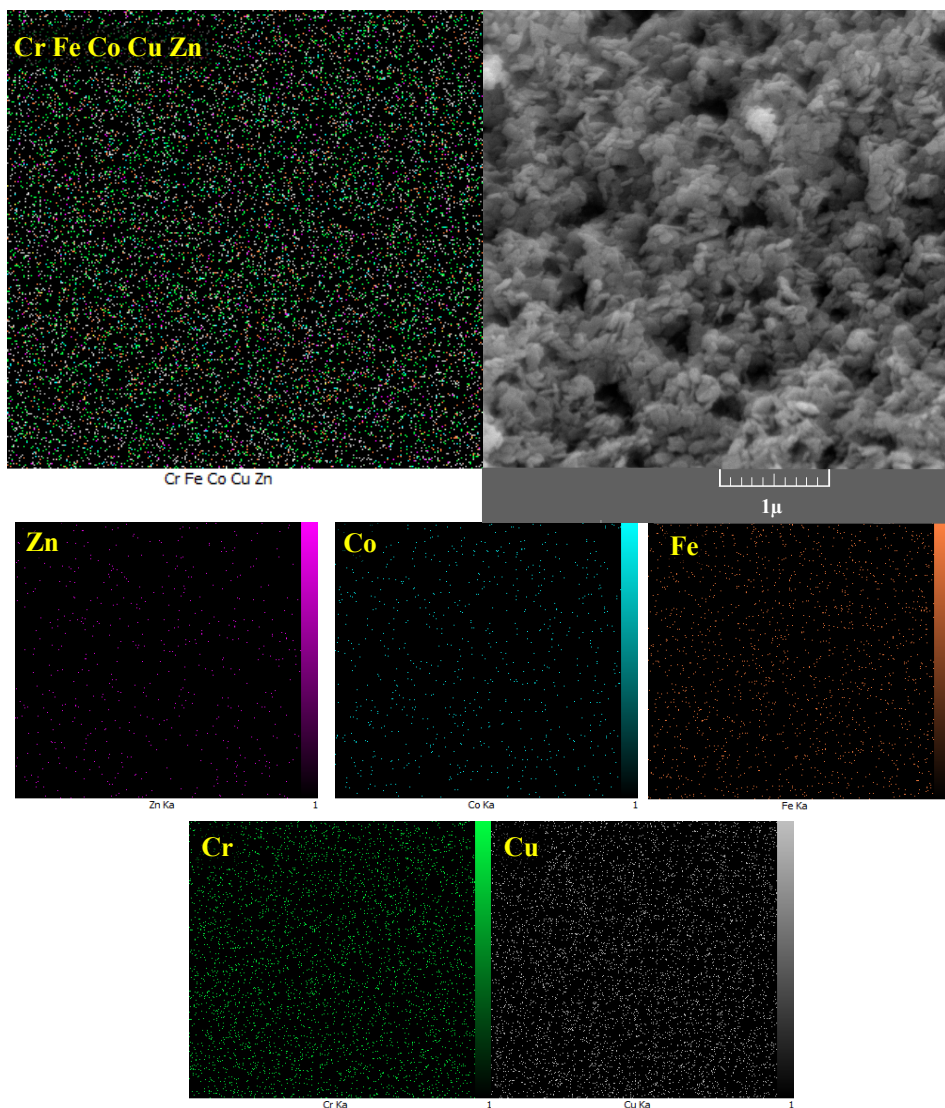


**Fig. 3.** SEM elemental mapping of the  $\text{Fe}_{2.5}\text{Co}_{0.3}\text{Zn}_{0.2}\text{O}_4/\text{CuCr-LDH}$ .

242

243

244

245 Furthermore, the surface area, the volume of gas adsorbed ( $V_m$ ) at standard temperature and

246 pressure, and pore volume extracted from the BET plot are inserted in Table 1. Accordingly,

247 the specific surface area of the composite was the largest, which in turn results in the higher

248 contribution of its surface in the photocatalytic degradation reactions. On the other hand,  $V_m$

249 was increased in the order of co-doped < LDH < composite, depicting the higher porosity of

250 the sample. Moreover, it should be noted that the obtained pore volume of the

251  $\text{Fe}_{2.5}\text{Co}_{0.2}\text{Zn}_{0.3}\text{O}_4/\text{CuCr-LDH}$  composite is relatively higher than those reported for other

252 composites such as NiFe-LDH/rGO (Khataee et al., 2019) and magnetic Mg-Fe/LDH

253 intercalated activated carbon (Alagha et al., 2020), which acknowledges the mesoporous  
254 characterization of the so-synthesized composite (Alagha et al., 2020).

255

256 **Table 1.** Textural properties of the so-synthesized samples extracted from the BET plot.

Samples	$S_{\text{BET}}$ ( $\text{m}^2 \text{g}^{-1}$ )	$V_{\text{m}}$ ( $\text{cm}^3 \text{(STP)} \text{g}^{-1}$ )	$V_{\text{P}}$ ( $\text{cm}^3 \text{g}^{-1}$ )
$\text{Fe}_{2.5}\text{Co}_{0.3}\text{Zn}_{0.2}\text{O}_4$	19.98	4.6	0.32
Pure CuCr-LDH	43.21	9.64	0.28
$\text{Fe}_{2.5}\text{Co}_{0.3}\text{Zn}_{0.2}\text{O}_4/\text{CuCr-LDH}$	74.21	17.21	0.39

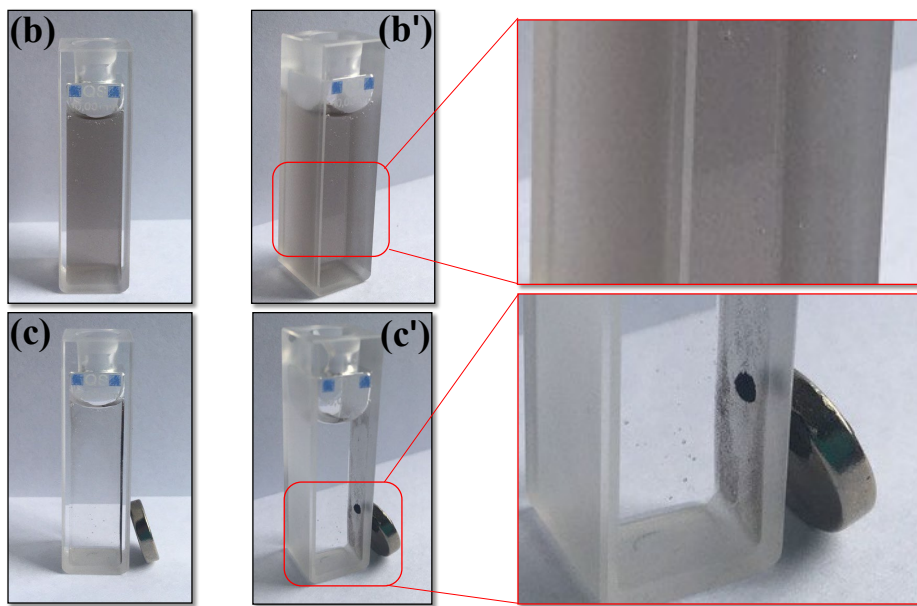
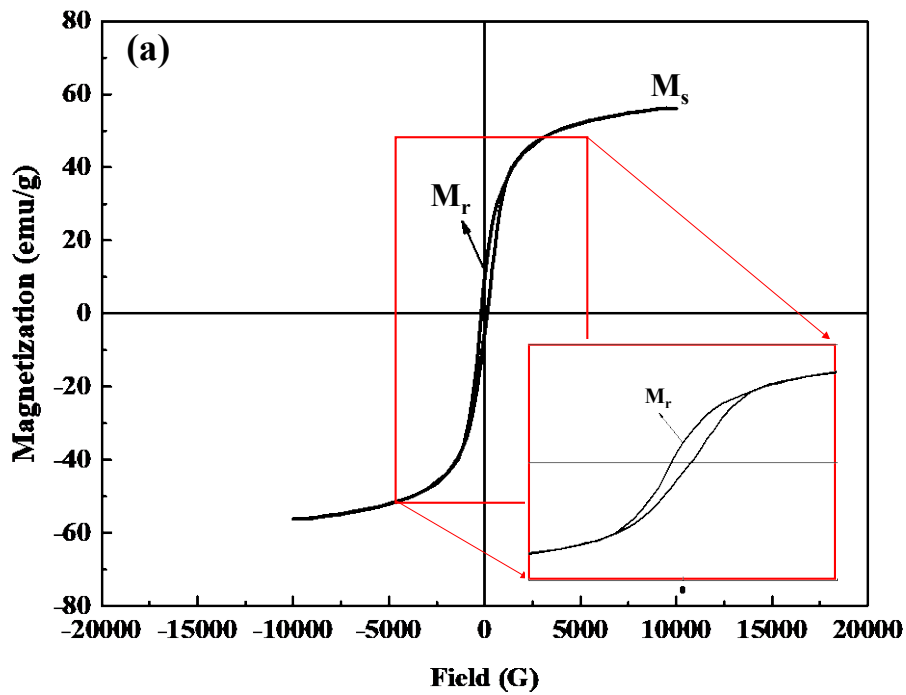
257

### 258 3.1.3. Optical and magnetic properties

259 To investigate the light response of the so-synthesized nanomaterials the UV-vis DRS  
260 analysis was applied. It was proved that the doped elements such as Co and Zn could modify  
261 the redox properties of the pure magnetite by preparing the oxygen vacancies in the magnetite  
262 structure which favors the electron capture (Fazli et al., 2021c). However, the prepared  
263 photocatalyst was not active under visible light irradiation. Considering Fig. S4, the composite  
264 of  $\text{Fe}_{2.5}\text{Co}_{0.3}\text{Zn}_{0.2}\text{O}_4$  nanoparticles with the CuCr-LDH enhanced the visible light absorption  
265 capacity. In conclusion, the effective light-absorbing capability of the composite could be  
266 aroused from two main facts: (I) the promoted photocatalytic efficiency of magnetite by doping  
267 Zn and Co metal ions to its structure, and (II) the inherent visible light absorption ability of  
268 CuCr-LDH compared to the magnetite nanoparticles could narrow the bandgap and raise the  
269 optical response of the final composite (Nguyen et al., 2021). The bandgap energies were  
270 estimated using the Kubelka-Monk formula and Tauc's plot (Rad et al., 2018). The  $(\alpha h\nu)^2$ - $h\nu$   
271 curves of the samples were displayed in Fig. S4. Using tangent line to the curves shown in Fig.  
272 S4, the bandgap of  $\text{Fe}_{2.5}\text{Co}_{0.3}\text{Zn}_{0.2}\text{O}_4$  nanoparticles, CuCr-LDH, and  $\text{Fe}_{2.5}\text{Co}_{0.3}\text{Zn}_{0.2}\text{O}_4/\text{CuCr-}$   
273 LDH composite was found to be 2.78, 2.69, and 1.66, respectively. The results confirmed the  
274 existence of a redshift in the absorbance spectrum of the composite which could be the main

275 role in its greater excitation under the visible light irradiation to generate reactive electron-hole.  
276 In our previous work (Fazli et al., 2021a), we realized that the combination of pure magnetite  
277 and layered double hydroxide results in the effective electron transfer on the surface of the  
278 composite leading to the lower recombination rate of the electron and holes. Consequently, the  
279 low bandgap as well as the efficient electron transfer on the surface of the  
280  $\text{Fe}_{2.5}\text{Co}_{0.3}\text{Zn}_{0.2}\text{O}_4/\text{CuCr-LDH}$  composite results in the increased production and availability of  
281 the electrons on its surface.

282 In our previous work, we observed that  $\text{Fe}_3\text{O}_4$  preserved its magnetic properties even after  
283 co-doping of Zn and Co in its structure (Fazli et al., 2021c). In addition, the magnetic properties  
284 of the prepared composite were evaluated by applying a systematic magnetization measuring  
285 as a function of the used field. Fig. 4 shows that the appraised value for the magnetization  
286 saturation ( $M_s$ ) of  $\text{Fe}_{2.5}\text{Co}_{0.3}\text{Zn}_{0.2}\text{O}_4/\text{CuCr-LDH}$  composite was  $56.14 \text{ emu g}^{-1}$ , indicating that  
287 the so-synthesized nanomaterial is a ferromagnetic phase (Kiziltaş et al., 2020). Hence, this  
288 magnetic behavior allowed the composite to be separated from the reaction media by applying  
289 an external magnetic field (inserted photo in Fig. 4).



290

291 **Fig.4.** (a) The VSM plot of the so-synthesized  $\text{Fe}_{2.5}\text{Co}_{0.3}\text{Zn}_{0.2}\text{O}_4/\text{CuCr-LDH}$  composite, the  
 292 front and side images of a spectrophotometer cell containing the suspension of  
 293  $\text{Fe}_{2.5}\text{Co}_{0.3}\text{Zn}_{0.2}\text{O}_4/\text{CuCr-LDH}$  composite before (b-b') and after (c-c') applying an external  
 294 magnetic field.

295

296 **3.2. Impact of different oxidation processes**



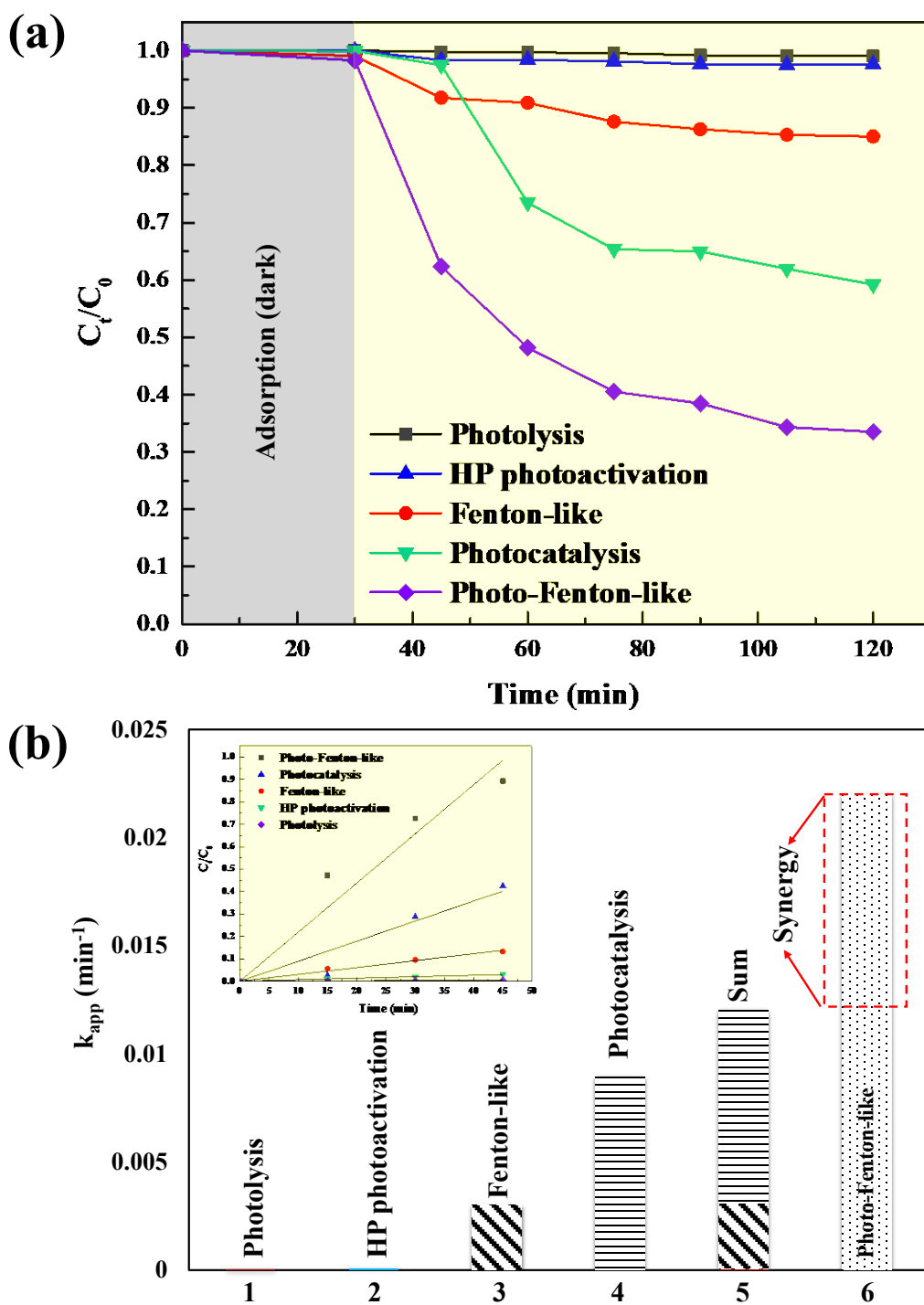
297 CAF was used as a model pollutant for evaluating the photo-Fenton-like degradation  
298 performance using  $\text{Fe}_{2.5}\text{Co}_{0.3}\text{Zn}_{0.2}\text{O}_4$ , CuCr-LDH, and  $\text{Fe}_{2.5}\text{Co}_{0.3}\text{Zn}_{0.2}\text{O}_4/\text{CuCr-LDH}$  composite  
299 under visible-light irradiation. Moreover, for better evaluation of their photocatalytic activity,  
300 the previously synthesized and characterized pure magnetite (Fazli et al., 2021c) and its  
301 composite with CuCr-LDH (Fazli et al., 2021a) was also used (Fig. S5). Before starting the  
302 photo-Fenton-like reactions, the adsorption trend of 50  $\mu\text{M}$  of CAF on the surface of the  
303 samples was studied. When the prepared solutions were stirred for 2 hours in the dark, the  
304 adsorption/desorption of CAF was equilibrated after 30 min (the results of 2 hours have not  
305 been reported). Therefore, in the case of stirring the solutions for 2h in the dark, the CAF  
306 adsorption percentage of 0.15, 2.46, 9.11, 0.05, and 2.7 % were achieved in the presence of  
307  $\text{Fe}_3\text{O}_4$ ,  $\text{Fe}_{2.5}\text{Co}_{0.3}\text{Zn}_{0.2}\text{O}_4$ , CuCr-LDH,  $\text{Fe}_3\text{O}_4/\text{CuCr-LDH}$ , and  $\text{Fe}_{2.5}\text{Co}_{0.3}\text{Zn}_{0.2}\text{O}_4/\text{CuCr-LDH}$   
308 composite, respectively. According to the results presented in Fig. S5, pure and co-doped  
309 magnetite have almost no response under the visible light irradiation for the CAF degradation.  
310 Also, the pure layered double hydroxide has shown more adsorption of CAF rather than its  
311 degradation. Considering the results obtained from the BET analysis, the main reason for high  
312 adsorption in the presence of the layered double hydroxide can be related to its higher surface  
313 area. However, combined adsorption and photo-Fenton-like processes reduced  $C_t/C_0$  of CAF,  
314 where the degradation efficiency was to be 41.6, and 66.4 % for  $\text{Fe}_3\text{O}_4/\text{CuCr-LDH}$ , and  
315  $\text{Fe}_{2.5}\text{Co}_{0.3}\text{Zn}_{0.2}\text{O}_4/\text{CuCr-LDH}$ , respectively. The higher degradation efficiency of CAF in the  
316 presence of  $\text{Fe}_{2.5}\text{Co}_{0.3}\text{Zn}_{0.2}\text{O}_4/\text{CuCr-LDH}$  composite is in line with the obtained results from the  
317 DRS analysis. The Low bandgap of the composite (1.66 eV), as well as, the presence of  
318 structural defects and metal-semiconductor interface (Schottky interface) in co-doped  
319 magnetite/LDH resulted in the higher production and better transference of electrons. This  
320 phenomenon led to the production of more hydroxyl radicals in the presence of HP (Cao et al.,  
321 2021). Our results followed the similar sequence obtained by the other researchers. For instance,

322 Cao et al (Cao et al., 2021). reported that the  $\text{La}_{0.7}\text{Sr}_{0.3}\text{MnO}_3/\alpha\text{-Fe}_2\text{O}_3$  composite possesses the  
323 best photocatalytic behavior in comparison with the pure  $\alpha\text{-Fe}_2\text{O}_3$  and  $\text{La}_{0.7}\text{Sr}_{0.3}\text{MnO}_3$ . Xiao et  
324 al (Xiao et al., 2020) also reported that the composite of Cu doping magnetite with Cu/C showed  
325 higher degradation efficiency for Rhodamine-B in comparison with the sole components.

326 As the  $\text{Fe}_{2.5}\text{Co}_{0.3}\text{Zn}_{0.2}\text{O}_4/\text{CuCr-LDH}$  composite resulted in high photo-Fenton-like oxidation  
327 of CAF, it was selected as the photocatalyst for evaluating CAF degradation under different  
328 degradation processes (Fig. 5) such as photolysis (just vis-light), HP photoactivation (HP/vis-  
329 light), Fenton-like (HP/composite), photocatalysis (vis-light/composite), photo-Fenton-like  
330 (HP/composite/vis-light). It is worth noting that CAF removal under dark conditions  
331 (adsorption) was lower than 2.7 %, therefore the related results have not been reported in Fig.  
332 5. No direct activation of HP under visible light irradiation was observed as expected, while the  
333 photocatalytic and Fenton-like processes raised the degradation rate of CAF to 40.8 and 14.9  
334 %, respectively. The results also confirmed that the presence of visible light resulted in the  
335 degradation efficiency of 3 times more than those for the sole Fenton-like process.

336 The enhanced degradation efficiency in the presence of the visible light source relates to the  
337 acceleration of  $\equiv\text{M(III)}/\equiv\text{M(II)}$  and  $\equiv\text{M(II)}/\equiv\text{M(I)}$  cycles by the contribution of photogenerated  
338 electrons coming from the excitation of the prepared semiconductor under visible light  
339 irradiation (Wu et al., 2020). This enhances the Fenton-like reactions for the production of  $\cdot\text{OH}$   
340 in the presence of HP. Palanivel et al, (Palanivel et al., 2019) proved that the nanocomposite of  
341  $\text{ZnFe}_2\text{O}_4$  and  $\text{g-C}_3\text{N}_4$  showed the existence of a synergistic effect for the appropriate degradation  
342 of Methylene blue in the presence of HP and under visible light irradiation. According to the  
343 authors, the high-performance photo-Fenton-like process had been resulted from the efficient  
344 separation of charge carriers and consequently more involvement of electrons in the  
345  $\equiv\text{Fe(III)}/\equiv\text{Fe(II)}$  cycle.

346



347  
 348 **Fig. 5.** Degradation of caffeine under different processes (a). Studying the synergistic effect  
 349 of photo-Fenton-like process using  $Fe_{2.5}Co_{0.3}Zn_{0.2}O_4/CuCr-LDH$  composite (b). Experimental  
 350 conditions: composite concentration of  $0.5 \text{ g L}^{-1}$ ,  $[caffeine] = 50 \mu\text{M}$ ,  $[H_2O_2 (HP)] = 5 \text{ mM}$   
 351 and  $\text{pH} = 8$ .

352

353 In the context of water pollutant degradation processes, the existence of a synergy factor is  
 354 essential (Fazli et al., 2021c). The synergy factor can be defined for those mixed degradation  
 355 processes which lead to a better degradation efficiency in comparison with the sum of individual  
 356 processes (Bansal and Verma, 2017). For this purpose, we studied the kinetics of CAF  
 357 degradation by applying the pseudo-first-order model ( $\ln \frac{C_0}{C_t} = k_{app} t$ ). The obtained correlation  
 358 coefficient values ( $R^2 > 0.9$ ) for all the processes reveal that the above-mentioned model fits  
 359 well for the degradation of CAF under the applied photo-Fenton-like process. The rate constants  
 360 ( $k_{app}$ ) for different processes have been reported in Table 2.

361

362 **Table 2.** The impact of various processes on the pseudo-first-order rate constants of caffeine  
 363 degradation.

<b>Processes</b>	<b><math>k_{app}</math> (min<sup>-1</sup>)</b>	<b>Correlation coefficient (R<sup>2</sup>)</b>
<b>Photolysis</b>	$4.1 \times 10^{-5}$	0.99
<b>Photoactivation of HP</b>	$5.7 \times 10^{-5}$	0.99
<b>Fenton-like</b>	0.003	0.99
<b>Photocatalysis</b>	0.008	0.95
<b>Photo-Fenton-like</b>	0.022	0.97

364

365 For studying in detail, a synergy factor (equation 1) was defined to determine the extent of  
 366 the synergy effect of the photo-Fenton-like process compared with the photolysis,  
 367 photoactivation of HP, Fenton-like, and photocatalytic processes. As a consequence, the  
 368 calculated synergy factor values for the photo-Fenton-like process were calculated to be 2.2,  
 369 verifying the enhancing performance in the integrated processes. In our previous work (Fazli et

370 al., 2021c), we also reported the synergistic effect of persulfate and HP activation using co-  
371 doped magnetite.

$$372 \quad R = \frac{k_{\text{app}}(\text{photo-Fenton-like})}{k_{\text{app}}(\text{photolysis}) + k_{\text{app}}(\text{HPphotoactivation}) + k_{\text{app}}(\text{Fenton-like}) + k_{\text{app}}(\text{photocatalysis})} \quad (1)$$

373

### 374 **3.3. Investigating the influential factors on CAF degradation**

375 Various factors such as the amount of composite, pH, HP concentration, and light source are  
376 known to have a significant effect on the Fenton-like and photo-Fenton-like processes (Fazli et  
377 al., 2021c). The composite concentration can have a positive or even reverse effect on the  
378 performance of different photocatalytic degradation processes (J. E. Yang et al., 2020).  
379 Therefore, the relationship between the composite concentration and CAF degradation was  
380 evaluated and the results were inserted in Fig. 6 (a). The increased composite concentration  
381 from 0.1 g L<sup>-1</sup> to 0.5 g L<sup>-1</sup> was accompanied by the enhanced degradation efficiency for CAF.  
382 It is assumed that the abundance of the active sites (J. E. Yang et al., 2020), as well as the  
383 generation of different reactive free radicals (Fazli et al., 2021a; Rad et al., 2018) in the reaction  
384 media, can be the major reason for the degradation of CAF. Nevertheless, beyond the observed  
385 increasing trend, the composite concentration of 0.75 g L<sup>-1</sup> and 1 g L<sup>-1</sup> displayed an obvious  
386 decline for the CAF degradation. In other terms, a higher increase in the amount of composite  
387 inhibited the performance of the photo-Fenton-like process. The results obtained by the other  
388 researchers are in good agreement with those of ours. Ghasemipour et al. (Ghasemipour et al.,  
389 2020) reported that in the case of using 0.7 g L<sup>-1</sup> of the RGO10%/ZnO20%/MoS<sub>2</sub> composite,  
390 the penetration of the utilized light to the surface of the composite decreased which was due to  
391 the fact that the reaction media had become opaque.

392 Since the solution pH is one of the crucial operating parameters affecting the Fenton-like  
393 and photo-Fenton-like reactions at the surface of the composite, we evaluated the effect of

394 different solution pHs on the degradation efficiency of CAF (Fig. 6 (b)). The results revealed  
395 that both strong acidic or basic solutions led to lower CAF degradation efficiency. Commonly,  
396 the Fenton-like reactions are more likely to occur in the lower pH values (Ye et al., 2021).  
397 However, the CAF degradation efficiency was observed to be low in very acidic conditions.  
398 Different researchers have also reported a lower performance of the photo-Fenton-like process  
399 in strong acidic conditions (Li et al., 2021; Xiaoliang Fan et al., 2021). Moreover, for basic  
400 solution, the lower degradation efficiency can be interpreted to I) the formation of less active  
401 structures such as  $\text{Fe}(\text{OH})_n$ , and II) the decomposition of HP to  $\text{O}_2$  and  $\text{H}_2\text{O}$  (Behrouzeh et al.,  
402 2020; Morshed et al., 2020). For basic solutions, This phenomenon restricts the production of  
403 different reactive species for the degradation of CAF reduces.

404 To better interpret the obtained results, the point of zero charges ( $\text{pH}_{\text{pzc}}$ ) was measured for  
405 the surface of the  $\text{Fe}_{2.5}\text{Co}_{0.3}\text{Zn}_{0.2}\text{O}_4/\text{CuCr-LDH}$  composite which is expressed in section (3-6-  
406 1) in details (Fig. S8). Based on the obtained results for  $\text{pH}_{\text{pzc}}$  and considering the protonated  
407 form of CAF in the lower pHs ( $\text{pH} < 10.4$ ) (Li et al., 2005a), the optimum degradation efficiency  
408 of CAF occurred at pH 8. Indeed, the repulsion force in  $\text{pH} < 6$  decreased the occurrence of  
409 degradation reactions on the surface of the composite. It is worth noting that in contrast to the  
410 homogenous photo-Fenton-like process, our proposed process showed higher performance for  
411 the degradation of CAF in the solution pH value of 8; hence, this pH value was selected as the  
412 optimum value for the subsequent test.

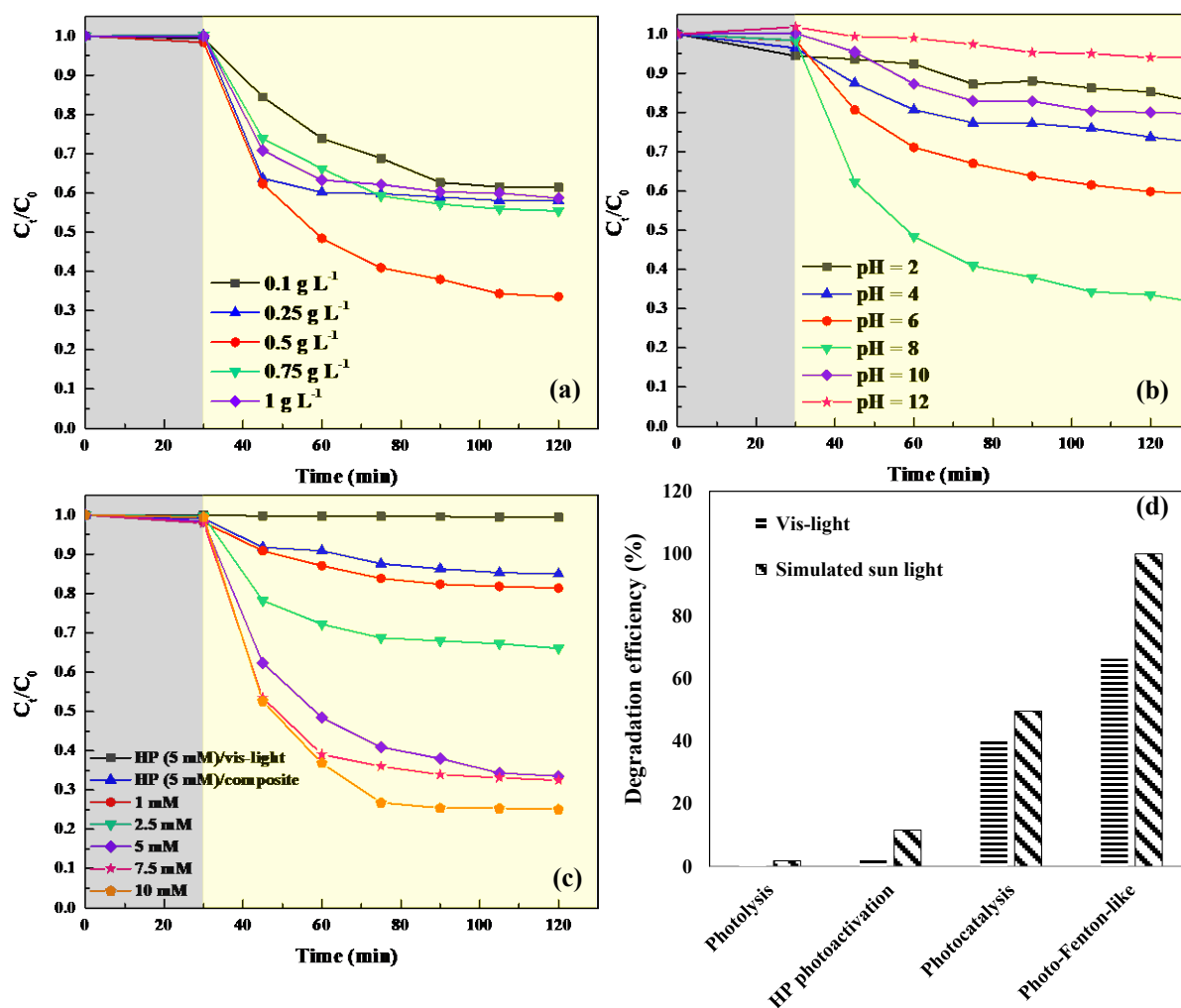
413 The impact of different HP concentrations on the degradation efficiency in the photo-Fenton-  
414 like process was also studied and the results were presented in Fig. 6 (c). From the results, it  
415 can be inferred that when more HP was introduced to the photo-Fenton-like process the  
416 degradation of CAF was accelerated. The increased degradation performance of the photo-  
417 Fenton-like process can be related to the fact that the composite was able to activate more  
418 amount of HP to generate reactive hydroxyl radicals for the degradation of the target pollutants.

419 However, further increase of HP concentration up to 7.5 and 10 mM didn't show a significant  
420 effect to accelerate the degradation efficiency of CAF under the optimal condition. Indeed,  
421 when the concentration of HP reaches its critical point, the performance of  $\cdot\text{OH}$  can be  
422 restricted by its reaction with the excessive amount of HP. The results obtained by Yang et al.  
423 (Yang et al., 2015) are in accordance with our results illustrated in Fig. 6 (c). They reported that  
424 the decomposition of methylene blue was enhanced by increasing the HP concentration from  
425 0.009 M to 0.176 M, whereas, further increasing it to 0.22 M demonstrated an adverse trend for  
426 the removal efficiency of methylene blue. To identify that the composite has the major effect  
427 on the degradation efficiency of CAF, 5 mM of HP was used for the degradation of CAF in the  
428 absence of photocatalyst and presence of the visible light. The results imply that the sole HP is  
429 not capable of CAF degradation, while the presence of composite and 5 mM of HP without vis-  
430 light brought about 15% of CAF degradation efficiency. Considering the factors mentioned  
431 above, we selected the HP concentration of 5 mM as the optimal concentration for the other  
432 tests.

433 Moreover, a set of experiments were fulfilled to assess the effect and contribution of different  
434 irradiating lights on the degradation efficiency of CAF during different processes. In this  
435 context, a simulated solar light was provided using a Xenon lamp with or without UV-cut-off  
436 filter ( $\lambda > 400$  nm). As it is clear from Fig. 6 (d), photolysis of CAF has not occurred in the  
437 presence of both light sources. Nonetheless, the presence of additional UV light in the simulated  
438 solar light enhanced the degradation efficiency of CAF from 2.2, 41.2, and 66.5 % (in the  
439 presence of vis-light) to 11.6, 50.1, and 100% for the HP photoactivation, photocatalysis, and  
440 photo-Fenton-like degradation processes, respectively. The principal reason for the enhanced  
441 degradation efficiency can be ascribed to the presence of UV fraction of the solar light (Li et  
442 al., 2018). Taking account of this fact, the so-synthesized photocatalyst can absorb available  
443 UV light, which in turn results in the generation of more electron-hole and subsequently more

444 reactive radical species. Therefore, the more reactive radical species produced in the reaction  
 445 media, the more CAF degradation achieved. Furthermore, not only can UV light activate HP to  
 446 produce more amount of  $\cdot\text{OH}$  (Gabet et al., 2021), it accelerates the reduction of Fe (III) into  
 447 Fe (II) (iron photolysis) as the essential agent for the Fenton-like reaction (Wu et al., 2020). Wu  
 448 et al. (Wu et al., 2020) compared the effect of visible and simulated solar light for the Fenton-  
 449 like degradation of tetracycline hydrochloride. Accordingly, they claimed that the existence of  
 450 UV light in the simulated solar light boosted the degradation efficiency of the target pollutant  
 451 from 34.5% to 78.3 %.

452



453  
 454 **Fig. 6.** The effect of (a) composite concentration, (b) initial pH, and (c) H<sub>2</sub>O<sub>2</sub> (HP)  
 455 concentration on the degradation efficiency of caffeine under photo-Fenton-like degradation



456 process. (d) The effect of different light sources on the performance of various processes.  
457 Experimental condition: composite concentration of 0.5 g L<sup>-1</sup>, [caffeine] = 50 μM, [H<sub>2</sub>O<sub>2</sub>] = 5  
458 mM and pH = 8.

459

### 460 **3.4. The stability and reusability of the photocatalyst**

461 The high photocatalytic activity, as well as a long-term stability of the composite, are the  
462 vital factors in the practical applications; hence, the reusability potential of the  
463 Fe<sub>2.5</sub>Co<sub>0.3</sub>Zn<sub>0.2</sub>O<sub>4</sub>/CuCr-LDH composite was tested in 5 cycles of recycling experiments for  
464 CAF degradation. According to the results depicted in Fig. S6 (inserted figure), the degradation  
465 efficiency of CAF from the first to 5<sup>th</sup> run decreased from 66.5 to 58.6%. Therefore, comparing  
466 with the first cycle, around a 10 % decrease in the CAF degradation efficiency was gained,  
467 revealing the persistence of composite stability. Our results in previous work (Fazli et al.,  
468 2021c) demonstrated that 5 cycles of the UVA/Fe<sub>2.5</sub>Co<sub>0.3</sub>Zn<sub>0.2</sub>O<sub>4</sub>/HP process resulted in a 10 %  
469 decrease in Sulfalene degradation efficiency. Yang et al. (Yang et al., 2015) reported that 99%  
470 of methylene blue was degraded in the cycle of the degradation process; however after six times  
471 of using the removal efficiency of the composite reduced to almost 90%.

472 The stability of the Fe<sub>2.5</sub>Co<sub>0.3</sub>Zn<sub>0.2</sub>O<sub>4</sub>/CuCr-LDH composite was further proved by  
473 comparing the XRD patterns of the freshly provided composite and the composite recycled after  
474 5 times of the degradation process (Fig. S6). The XRD patterns illustrated that the so-  
475 synthesized composite did not undergo significant structural variation even after five times of  
476 usage. This fact was further verified by ICP analysis, which was applied to determine the  
477 concentration of dissolved metal ions from the utilized composite in solution pH of 8.  
478 Interestingly, the released concentration of Fe, Co, Zn, Cu, and Cr was attained to be 1.8 μg L<sup>-1</sup>,  
479 2.1 μg L<sup>-1</sup>, 1.5 μg L<sup>-1</sup>, 1.7 μg L<sup>-1</sup>, and 1.2 μg L<sup>-1</sup>, respectively. The achieved results were  
480 found to be lower than the standard value reported by the World Health Organization (WHO)

481 (Fazli et al., 2021c, 2021a), indicating the excellent stability of the Fe<sub>2.5</sub>Co<sub>0.3</sub>Zn<sub>0.2</sub>O<sub>4</sub>/CuCr-  
482 LDH composite during the applied degradation process. Therefore, our findings affirmed that  
483 the Fe<sub>2.5</sub>Co<sub>0.3</sub>Zn<sub>0.2</sub>O<sub>4</sub>/CuCr-LDH composite is a stable photocatalyst, which can be used  
484 continually in extended environmental applications.

485

### 486 **3.5. The effect of inorganic anions and radical scavengers**

487 The existence of different inorganic ions in natural water and wastewater can interfere with  
488 the oxidation process of various water contaminants. In this context, different concentrations of  
489 chloride and bicarbonate were used to identify their inhibitory impact on the photo-Fenton-like  
490 degradation of CAF. As it is clear from Fig. S7 (a), in the case of using 5 and 10 mM of Cl<sup>-</sup> a  
491 slight decrease (4% and 9%, respectively) in the degradation efficiency of CAF was observed.  
492 This effect can be explained considering the complex reaction system starting from the reaction  
493 between <sup>•</sup>OH and Cl<sup>-</sup> (reactions 1 to 3). In fact, the formation of less oxidant species such as  
494 dichloride radical anion Cl<sub>2</sub><sup>•-</sup> is only favored under acidic conditions (reaction 2) (Huang et al.,  
495 2018a; Khataee et al., 2018).



499 HCO<sub>3</sub><sup>-</sup> is one of the other effective radical scavengers that can convert the highly active  
500 hydroxyl radicals to carbonate radicals (CO<sub>3</sub><sup>•-</sup>) (reaction 4).

501



503 In fact, when we used different concentrations of HCO<sub>3</sub><sup>-</sup> ions in the photo-Fenton-like the  
504 CAF degradation efficiency was reduced from 66.5% to 58.9% and 52.8% using 5 and 10 mM

505 of  $\text{HCO}_3^-$ , respectively. Moreover, our results elucidated that in comparison with chloride the  
506  $\text{HCO}_3^-$  ions have a slightly stronger inhibiting effect on the degradation of CAF. Liu et al. (Liu  
507 et al., 2020) studied the effect of 10 mM of chloride and bicarbonate in the photo-Fenton-like  
508 degradation of nitrobenzene in the presence of 8 mM of HP and UV light. They also reported  
509 that in comparison with the  $\text{Cl}^-$  ions, 10 mM of  $\text{HCO}_3^-$  showed a more inhibiting effect on the  
510 degradation of nitrobenzene. Wu et al. (Wu et al., 2017) studied the effect of bicarbonate in the  
511 degradation of 4-tert-butylphenol in the course of persulfate activation by Fe (III) species at the  
512 solution pH of 8. According to their results, the presence of 2 and 10 mM of bicarbonate resulted  
513 in the complete inhibition of 4-tert-butylphenol degradation. Moreover, Tao et al. (Tao et al.,  
514 2021) studied the degradation of phenantrene by using UVB activation of hydrogen peroxide.  
515 They have also studied the effect of bicarbonate on the phenantrene degradation. According to  
516 their results, in the presence of 50 mM of bicarbonate, phenantrene concentration of  $10 \text{ mg L}^{-1}$ ,  
517 and at pH of 8, the degradation efficiency of phenantrene was decreased from 33% to almost  
518 16%, indicating a great inhibiting effect of bicarbonate in the presence of homogenous  
519 activation of hydrogen peroxide. Heung et al. (Huang et al., 2018b) reported a 50% inhibition  
520 of bisphenol A in the presence of 5mM of carbonates and UV- $\text{H}_2\text{O}_2$  process. Therefore, it is  
521 evident that bicarbonate showed a lower inhibiting effect on CAF during our applied photo-  
522 Fenton-like process.

523 Different scientists such as He et al. reported that  $\bullet\text{OH}$ , superoxide anion radical ( $\text{O}_2^{\bullet-}$ ), and  
524 photo-generated electron-hole are the primary active species that are responsible for the  
525 degradation of organic pollutants through the photo-Fenton-like process. In this regard,  
526 isopropanol alcohol (IPA), 4-hydroxy-2,2,6,6-tetramethylpiperidin-1-oxyl (Tempol),  
527 chloroform, and KI have been widely used as the appropriate radical scavenger for  $\bullet\text{OH}$ ,  $\text{O}_2^{\bullet-}$ ,  
528 and photogenerated electron and holes, respectively (Fazli et al., 2021c; Jing et al., 2021;  
529 Shyamala and Gomathi Devi, 2020). The degradation efficiency of CAF was evaluated in the

530 absence and presence of the abovementioned radical inhibitors and the results were  
531 demonstrated in Fig. S7 (b). Owing to the obtained results, an obvious reduction of CAF  
532 degradation efficiency was observed in the presence of IPA, which reveals the participation of  
533 reactive  $\cdot\text{OH}$  in the CAF decomposition. Also, to avoid the probable reaction of  $\cdot\text{OH}$  with  
534 other radical scavengers, IPA with its much higher second-order reaction rate constant ( $k_{\cdot\text{OH}}$   
535  $= 1.6 \times 10^9 \text{ M}^{-1} \text{ s}^{-1}$ ) (Jin et al., 2018) were used in all the following experiments. Therefore, the  
536 presence of IPA and tempol brought about an additional 13.5% inhibition in the CAF  
537 degradation, which can be effectively ascribed to the contribution of  $\text{O}_2^{\bullet-}$ . On the other hand,  
538 chloroform has been reported to react with both  $\text{O}_2^{\bullet-}$  and photogenerated electrons ( $k_{\text{O}_2^{\bullet-}}$   
539  $= 2.8 \times 10^8 \text{ M}^{-1} \text{ s}^{-1}$  and  $k_{e^-} = 3 \times 10^{10} \text{ M}^{-1} \text{ s}^{-1}$ ) (Guo et al., 2021). The holes were capture by the  
540 available iodide ion and resulted in decreased degradation extent. However, to remove the  
541 possible reaction between chloroform and superoxide or hydroxyl radicals, this experiment has  
542 been fulfilled in the presence of tempol and IPA. The reduction was found to be approximately  
543 10.6 %. Chloroform was used to study the participation of photogenerated electrons in the  
544 degradation efficiency of CAF. The results showed less contribution of the photogenerated  
545 electrons in the decomposition of CAF. Consequently, the active impact of the reactive species  
546 can be denoted in the following raising order:  $\cdot\text{OH} > \text{O}_2^{\bullet-} > \text{h}^+ > \text{e}^-$ . The obtained results were  
547 similar to the research conducted by Abdelhaleem (Abdelhaleem and Chu, 2020) et al., which  
548 used a  $\text{Fe}^{\text{III}}$  impregnated N-TiO<sub>2</sub>/HP/visible LED process for the degradation of a pesticide  
549 (Carbofuran) from water. They also found out that the photo-Fenton-like degradation process  
550 in the presence of Fe (III) impregnated N-TiO<sub>2</sub> resulted in more production and contribution of  
551  $\cdot\text{OH}$  in the Carbofuran degradation.

552

### 553 **3.6. Simultaneous degradation of different water pollutants**

554 The effectiveness of the degradation process for the decomposition of different kinds of  
555 organic pollutants is of great importance for different scientists (Chavan and Fulekar, 2020;  
556 Rimoldi et al., 2017a). Therefore, we studied the photo-Fenton-like degradation of pollutants  
557 mixture. With respect to the literature review, BPA and SIM have been classified as water  
558 contaminants that are able to create health disorders (Jiang et al., 2020; Sahu et al., 2021).  
559 Therefore, besides caffeine as the pharmaceutical water pollution, BPA and SIM were also used  
560 as industry and herbicide contaminants. The detailed information of the compounds was given  
561 in Table S1.

562

### 563 **3.6.1. Degradation and mineralization of pollutants mixture**

564 The dark adsorption curves of three target pollutants at the pre-irradiated composite surface  
565 illustrated that adsorption/desorption equilibrium was reached less than 5% in 30 min (results  
566 were not shown in Fig. 7). Besides, Fig. 7 (a) demonstrates the degradation of pollutants mixture  
567 under the photo-Fenton-like degradation process. The results depicted that, the degradation  
568 efficiencies of three organic pollutants (SIM, CAF, and BPA) with the total concentration of 25  
569  $\mu\text{M}$  were found to be almost 52, 48, and 37 %, respectively. Therefore, the utilized process was  
570 found to be more effective for the degradation of SIM and CAF in comparison with BPA. The  
571 reason can be ascribed to the reactions which take place on the surface of the composite. With  
572 respect to the obtained  $\text{pH}_{\text{pzc}} = 5.9$  for the composite (Fig. S8), in the case of a greater pH value  
573 of the solution ( $\text{pH} > \text{pH}_{\text{pzc}}$ ), the surface would be saturated with the negative charge, while in  
574 the acidic solution ( $\text{pH} < \text{pH}_{\text{pzc}}$ ) the surface of the composite would be stuffed with the positive  
575 charges (Fazli et al., 2021c). Besides, the dissociation constant ( $\text{pK}_{\text{a}}$ ) of CAF, BPA, and SIM  
576 (Lee et al., 2020, p. 4; Li et al., 2005b) have been presented in Fig. S8. Thus, for the solution  
577 pH of 8, the surface of the composite is negative which can attract the protonated CAF and the  
578 least soluble SIM ( $6.2 \text{ mg L}^{-1}$ ) toward the surface of the composite. In the research study  
579 belonging to Rimoldi et al. (Rimoldi et al., 2017b), similar results were achieved. They studied

580 the photocatalytic degradation of the mixture containing tetracycline, caffeine, paracetamol,  
581 and atenolol in the presence of TiO<sub>2</sub>. They reported that among the available pollutants poorly  
582 soluble tetracycline showed a higher rate of photocatalytic degradation.

583 The effect of the photo-Fenton-like process on the mineralization of pollutants mixture was  
584 investigated with the aim to study the fate of the produced intermediates in the treated water.  
585 In this context, an experiment was conducted in the predetermined optimum condition and the  
586 TOC removal was reported. The efficiency of the photo-Fenton-like degradation process in  
587 terms of the TOC removal for the pollutants mixture was found to be ~ 68% after 4 h of process,  
588 respectively. Therefore, the photo-Fenton-like process in the presence of the  
589 Fe<sub>2.5</sub>Co<sub>0.3</sub>Zn<sub>0.2</sub>O<sub>4</sub>/CuCr-LDH composite can be determined as the reliable process for the  
590 degradation and long-term mineralization of the pollutants mixture in the solution pH close to  
591 the real wastewater. Ghasemipour et al. in their study on the photocatalytic degradation of  
592 Aniline reported that at pH solution of 4, and the RGO10%/ZnO20%/MoS<sub>2</sub> concentration of  
593 0.7 g L<sup>-1</sup>, the TOC removal of 40% over the time of 120 min (Ghasemipour et al., 2020). They  
594 also reported that more TOC removal of the pollutants mixture was obtained during the longer  
595 photocatalytic degradation process.

596

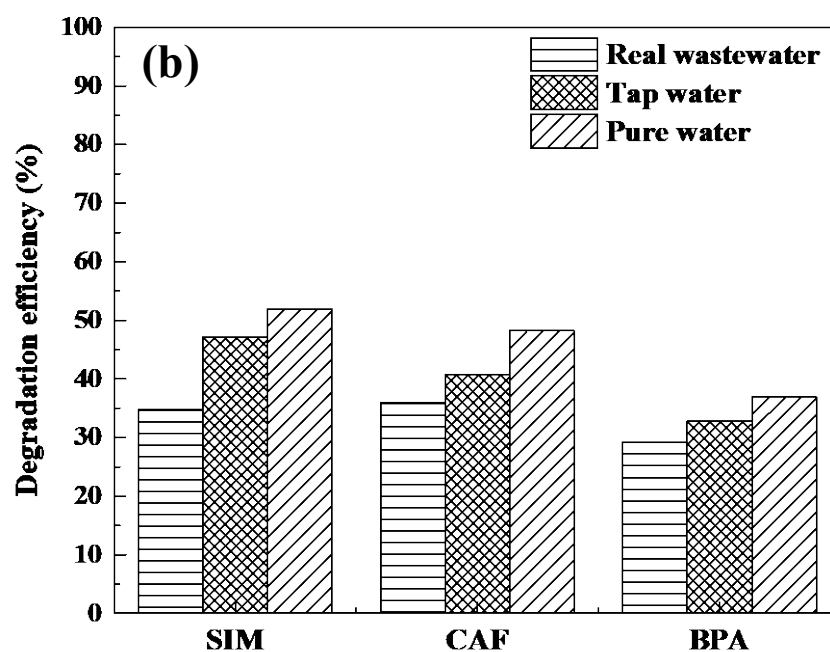
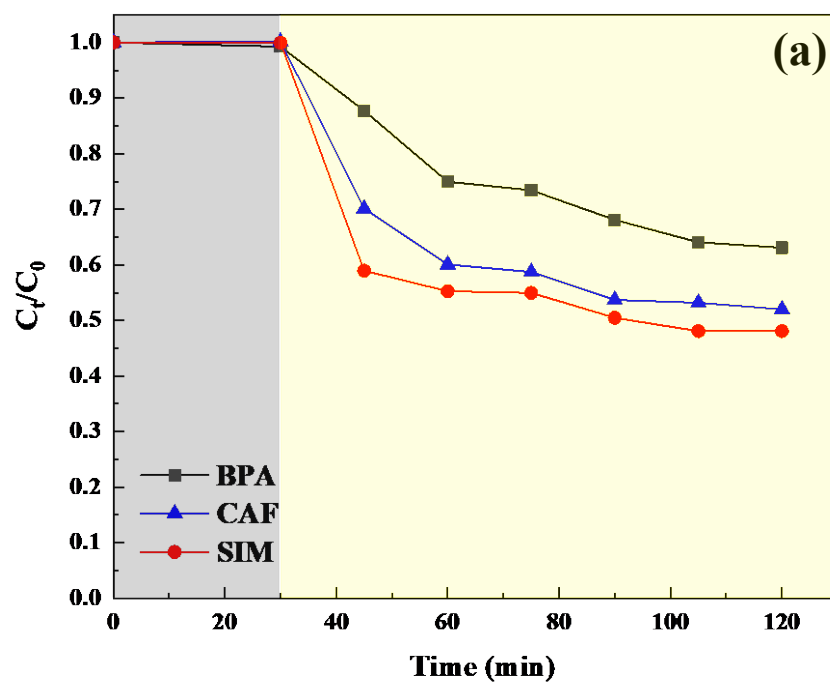
### 597 **3.6.2. Degradation of pollutants mixture in different water bodies**

598 In order to study whether the applied photo-Fenton-like process is suitable for practical  
599 purposes, the degradation of the pollutant was assessed in different water types. In this regard,  
600 we prepared the pollutants mixture solutions in the ultra-pure water, tap water from the  
601 University Clermont Auvergne, and real wastewater obtained from the municipal wastewater  
602 treatment plant of the Metropole of Clermont-Ferrand, France. The results presented in Fig. 7  
603 (b) show that various water matrix resulted in quite different degradation efficiency. A decline  
604 in the degradation efficiency of the pollutants in tap water can be related to the inhibition of

605 produced  $\cdot\text{OH}$  by  $\text{HCO}_3^-$  (2.35 mM) that are present in this kind of water. Not only can the  
606 hydrogenocarbonate anions occupy the active sites of the photocatalysts to reduce the  
607 production of ROS, but also they react with the produced hydroxyl radicals and convert them  
608 to the lower oxidative species (reaction 4).

609 Moreover, Fig. 7 (b) exhibits the accurate comparison for the effect of wastewater matrix on  
610 the degradation of three target pollutants. Over 120 min of the process and in the real  
611 wastewater, the degradation efficiencies of 34.8%, 36.0%, and 29.2% were respectively found  
612 for each of SIM, CAF, and BPA from their mixture solution. The reason for lower efficiency  
613 in comparison with those obtained in tap and ultra-pure water mainly depends on the presence  
614 of organic matter and inorganic compounds in the real wastewater, which can compete with the  
615 available reactive oxygen species such as hydroxyl radical, superoxide radical anion, and photo-  
616 generated electron and hole. However, the results undoubtedly show that in the real wastewater,  
617 the photo-Fenton-like process in the presence of  $\text{Fe}_{2.5}\text{Co}_{0.3}\text{Zn}_{0.2}\text{O}_4/\text{CuCr-LDH}$  composite can  
618 degrade more than 30 % of each three water contaminants from their mixture solution, which  
619 is good evidence for the efficiency of the proposed performance for the degradation of a wide  
620 range of pollutants in the wastewater. Ouyang et al. (Ouyang et al., 2020) declared the same  
621 consequence in their research work. They reported that the existence of diverse inorganic and  
622 organic substances in the acrylonitrile wastewater reduced the activity of the composite and the  
623 generated reactive species during photocatalytic degradation.

624



625  
 626 **Fig. 7.** (a) The adsorption and degradation of simazine (SIM), caffeine (CAF), and bisphenol  
 627 A (BPA) from their mixture solution in pure water, (b) the effect of different water types on  
 628 the degradation efficiency of pollutants in their mixture after 120 min of the process.  
 629 Experimental condition: composite concentration of  $0.5 \text{ g L}^{-1}$ , total pollutant concentration of  
 630  $25 \text{ } \mu\text{M}$ ,  $[\text{H}_2\text{O}_2] = 5 \text{ mM}$ , and  $\text{pH} = 8$ .

631



## 632 **Conclusion**

633 In this research, a  $\text{Fe}_{2.5}\text{Co}_{0.3}\text{Zn}_{0.2}\text{O}_4/\text{CuCr-LDH}$  composite with a well-defined structure was  
634 synthesized with a co-precipitation method and its photocatalytic activity was compared with  
635 those for  $\text{Fe}_3\text{O}_4$ , CuCr-LDH,  $\text{Fe}_{2.5}\text{Co}_{0.3}\text{Zn}_{0.2}\text{O}_4$ ,  $\text{Fe}_3\text{O}_4/\text{CuCr-LDH}$  photocatalysts. Thereafter,  
636 the synergistic effect of the photo-Fenton-like process for the degradation of an individual  
637 pollutant (CAF) was assessed. Furthermore, a set of experiments were fulfilled to study the  
638 effect of different composite concentrations, initial pH, HP concentration, and light sources  
639 were evaluated. Accordingly, almost 67% of CAF was degraded in the presence of  $0.5 \text{ g L}^{-1}$   
640 composite concentration, HP (5mM), and at initial solution pH of 8. It was also observed that  
641 the used composite preserved its structure and stability even after 5 cycles of successive  
642 reactions and it was possible to separate it from the reaction media by applying an external  
643 magnetic field. Moreover, in the presence of a simulated solar light without a UV cut-off filter,  
644 the degradation efficiency was raised to be 100%. Comparing our results with those published  
645 on homogenous photo-Fenton processes, chloride and bicarbonate showed lower inhibiting  
646 effects on the degradation of CAF, which is an encouraging result for the future application.  
647 Given the results obtained in the presence of different radical scavengers  $\cdot\text{OH}$  was found to  
648 contribute more to the photo-Fenton-like degradation of CAF. In addition, the mixture of CAF,  
649 SIM, and BPA was subjected to the photo-Fenton-like degradation process to study their  
650 removal efficiency. The TOC removal test depicted the existence of 68% TOC removal of  
651 pollutants mixture after 4h of the photo-Fenton-like degradation process. This confirms the  
652 complete conversion of the compounds to harmless compounds. Finally, the degradation of a  
653 mixture of three contaminates was also investigated in the tap and real wastewater. Although  
654 the probable impurities existing in the tap and wastewater reduced the degradation efficiency  
655 of the pollutants, more than 30% removal efficiency was achieved for each of the pollutants (>  
656 90 % for total pollutants mixture). In a conclusion, this work shows the feasibility of developing

657 new visible-light-responsive photocatalysts which reduces the limitation of AOPs such as their  
658 pH-dependence, high cost, and generation of secondary pollution with the catalysts.

659

## 660 **Acknowledgments**

661 We acknowledge the French Embassy in Iran, the project I-Site CAP 20-25, the program  
662 PAUSE of collège de France, and PAI (Pack Ambition Recherche internationale) SOLDE from  
663 the Region Auvergne Rhône Alpes for the financial support of Arezou Fazli in this project.  
664 Moreover, we would like to thank the Scientific and Technical Research Council of Turkey  
665 (TUBITAK, Project Number: 120Y350) for the financial support of the research project. The  
666 authors are thankful to Mhammed Banbakkar for conducting the ICP analysis and Dr.  
667 Guillaume Monier for accomplishing the XPS analysis.

668

669

670

671

672 **References**

- 673 Abdelhaleem, A., Chu, W., 2020. Prediction of carbofuran degradation based on the hydroxyl  
674 radical's generation using the FeIII impregnated N doped-TiO<sub>2</sub>/H<sub>2</sub>O<sub>2</sub>/visible LED  
675 photo-Fenton-like process. *Chem. Eng. J.* 382, 122930.  
676 <https://doi.org/10.1016/j.cej.2019.122930>
- 677 Aghaziarati, M., Yamini, Y., Shamsayei, M., 2020. An electrodeposited terephthalic acid-  
678 layered double hydroxide (Cu-Cr) nanosheet coating for in-tube solid-phase  
679 microextraction of phthalate esters. *Microchim. Acta* 187, 118.  
680 <https://doi.org/10.1007/s00604-019-4102-5>
- 681 Alagha, O., Manzar, M.S., Zubair, M., Anil, I., Mu'azu, N.D., Qureshi, A., 2020. Magnetic Mg-  
682 Fe/LDH Intercalated Activated Carbon Composites for Nitrate and Phosphate Removal  
683 from Wastewater: Insight into Behavior and Mechanisms. *Nanomaterials* 10, 1361.  
684 <https://doi.org/10.3390/nano10071361>
- 685 Bai, J., Liu, Y., Yin, X., Duan, H., Ma, J., 2017. Efficient removal of nitrobenzene by Fenton-  
686 like process with Co-Fe layered double hydroxide. *Appl. Surf. Sci.* 416, 45–50.  
687 <https://doi.org/10.1016/j.apsusc.2017.04.117>
- 688 Bansal, P., Verma, A., 2017. Synergistic effect of dual process (photocatalysis and photo-  
689 Fenton) for the degradation of Cephalexin using TiO<sub>2</sub> immobilized novel clay beads  
690 with waste fly ash/foundry sand. *J. Photochem. Photobiol. Chem.* 342, 131–142.  
691 <https://doi.org/10.1016/j.jphotochem.2017.04.010>
- 692 Behrouzeh, M., Abbasi, M., Osfouri, S., Dianat, M.J., 2020. Treatment of DMSO and DMAC  
693 wastewaters of various industries by employing Fenton process: Process performance  
694 and kinetics study. *J. Environ. Chem. Eng.* 8, 103597.  
695 <https://doi.org/10.1016/j.jece.2019.103597>

696 Brillas, E., 2020. A review on the photoelectro-Fenton process as efficient electrochemical  
697 advanced oxidation for wastewater remediation. Treatment with UV light, sunlight, and  
698 coupling with conventional and other photo-assisted advanced technologies.  
699 *Chemosphere* 250, 126198. <https://doi.org/10.1016/j.chemosphere.2020.126198>

700 Cao, X.-F., Yue, P., Wei, Q.-R., Dang, Y.-F., Zhang, S.-Q., Wei, Z.-X., Wang, R.-Z., 2021.  
701 Synthesis, characterization and catalytic performance of magnetic  $\text{La}_{0.7}\text{Sr}_{0.3}\text{MnO}_3/\alpha\text{-Fe}_2\text{O}_3$   
702 with p-n heterojunction structure. *J. Mater. Sci.* 56, 7862–7878.  
703 <https://doi.org/10.1007/s10853-021-05788-3>

704 Chavan, A., Fulekar, M.H., 2020. Enhanced degradation efficiency of mixed industrial effluent  
705 by modified nanocomposite photocatalyst under UVLED irradiation. *Nanotechnol.*  
706 *Environ. Eng.* 5, 5. <https://doi.org/10.1007/s41204-020-0069-z>

707 Chen, F., Huang, G.-X., Yao, F.-B., Yang, Q., Zheng, Y.-M., Zhao, Q.-B., Yu, H.-Q., 2020.  
708 Catalytic degradation of ciprofloxacin by a visible-light-assisted peroxymonosulfate  
709 activation system: Performance and mechanism. *Water Res.* 173, 115559.  
710 <https://doi.org/10.1016/j.watres.2020.115559>

711 Chen, H., Hu, L., Chen, M., Yan, Y., Wu, L., 2014. Nickel–Cobalt Layered Double Hydroxide  
712 Nanosheets for High-performance Supercapacitor Electrode Materials. *Adv. Funct.*  
713 *Mater.* 24, 934–942. <https://doi.org/10.1002/adfm.201301747>

714 Chen, R., Jiang, H., Li, Y.-Y., 2018. Caffeine degradation by methanogenesis: Efficiency in  
715 anaerobic membrane bioreactor and analysis of kinetic behavior. *Chem. Eng. J.* 334,  
716 444–452. <https://doi.org/10.1016/j.cej.2017.10.052>

717 Fazli, A., Brigante, M., Khataee, A., Mailhot, G., 2021a. Synthesis of a magnetically separable  
718 LDH-based S-scheme nano-heterojunction for the activation of peroxymonosulfate  
719 towards the efficient visible-light photodegradation of diethyl phthalate. *Appl. Surf. Sci.*  
720 149906. <https://doi.org/10.1016/j.apsusc.2021.149906>

721 Fazli, A., Khataee, A., Brigante, M., Mailhot, G., 2021b. Cubic cobalt and zinc co-doped  
722 magnetite nanoparticles for persulfate and hydrogen peroxide activation towards the  
723 effective photodegradation of Sulfalene. *Chem. Eng. J.* 404, 126391.  
724 <https://doi.org/10.1016/j.cej.2020.126391>

725 Gabet, A., Métivier, H., de Brauer, C., Mailhot, G., Brigante, M., 2021. Hydrogen peroxide and  
726 persulfate activation using UVA-UVB radiation: Degradation of estrogenic compounds  
727 and application in sewage treatment plant waters. *J. Hazard. Mater.* 405, 124693.  
728 <https://doi.org/10.1016/j.jhazmat.2020.124693>

729 Ghasemipour, P., Fattahi, M., Rasekh, B., Yazdian, F., 2020. Developing the Ternary ZnO  
730 Doped MoS<sub>2</sub> Nanostructures Grafted on CNT and Reduced Graphene Oxide (RGO) for  
731 Photocatalytic Degradation of Aniline. *Sci. Rep.* 10, 4414.  
732 <https://doi.org/10.1038/s41598-020-61367-7>

733 Gonçalves, R.G.L., Lopes, P.A., Resende, J.A., Pinto, F.G., Tronto, J., Guerreiro, M.C., de  
734 Oliveira, L.C.A., de Castro Nunes, W., Neto, J.L., 2019. Performance of  
735 magnetite/layered double hydroxide composite for dye removal via adsorption, Fenton  
736 and photo-Fenton processes. *Appl. Clay Sci.* 179, 105152.  
737 <https://doi.org/10.1016/j.clay.2019.105152>

738 Guo, Y., Zhang, Y., Yu, G., Wang, Y., 2021. Revisiting the role of reactive oxygen species for  
739 pollutant abatement during catalytic ozonation: The probe approach versus the  
740 scavenger approach. *Appl. Catal. B Environ.* 280, 119418.  
741 <https://doi.org/10.1016/j.apcatb.2020.119418>

742 Hieu, V.Q., Phung, T.K., Nguyen, T.-Q., Khan, A., Doan, V.D., Tran, V.A., Le, V.T., 2021.  
743 Photocatalytic degradation of methyl orange dye by Ti<sub>3</sub>C<sub>2</sub>-TiO<sub>2</sub> heterojunction under  
744 solar light. *Chemosphere* 276, 130154.  
745 <https://doi.org/10.1016/j.chemosphere.2021.130154>

746 Huang, W., Bianco, A., Brigante, M., Mailhot, G., 2018a. UVA-UVB activation of hydrogen  
747 peroxide and persulfate for advanced oxidation processes: Efficiency, mechanism and  
748 effect of various water constituents. *J. Hazard. Mater.* 347, 279–287.  
749 <https://doi.org/10.1016/j.jhazmat.2018.01.006>

750 Jiang, C., Yang, Y., Zhang, L., Lu, D., Lu, L., Yang, X., Cai, T., 2020. Degradation of Atrazine,  
751 Simazine and Ametryn in an arable soil using thermal-activated persulfate oxidation  
752 process: Optimization, kinetics, and degradation pathway. *J. Hazard. Mater.* 400,  
753 123201. <https://doi.org/10.1016/j.jhazmat.2020.123201>

754 Jin, Y., Sun, S.-P., Yang, X., Chen, X.D., 2018. Degradation of ibuprofen in water by FeII-  
755 NTA complex-activated persulfate with hydroxylamine at neutral pH. *Chem. Eng. J.*  
756 337, 152–160. <https://doi.org/10.1016/j.cej.2017.12.094>

757 Jing, L., Wang, D., He, M., Xu, Y., Xie, M., Song, Y., Xu, H., Li, H., 2021. An efficient broad  
758 spectrum-driven carbon and oxygen co-doped g-C<sub>3</sub>N<sub>4</sub> for the photodegradation of  
759 endocrine disrupting: Mechanism, degradation pathway, DFT calculation and toluene  
760 selective oxidation. *J. Hazard. Mater.* 401, 123309.  
761 <https://doi.org/10.1016/j.jhazmat.2020.123309>

762 Khataee, A., Fazli, A., Fathinia, M., Vafaei, F., 2018. Removal of diatom *Nitzschia* sp. cells via  
763 ozonation process catalyzed by martite nanoparticles. *J. Clean. Prod.* 186, 475–489.  
764 <https://doi.org/10.1016/j.jclepro.2018.03.136>

765 Khataee, A., Sadeghi Rad, T., Nikzat, S., Hassani, A., Aslan, M.H., Kobya, M., Demirbaş, E.,  
766 2019. Fabrication of NiFe layered double hydroxide/reduced graphene oxide (NiFe-  
767 LDH/rGO) nanocomposite with enhanced sonophotocatalytic activity for the  
768 degradation of moxifloxacin. *Chem. Eng. J.* 375, 122102.  
769 <https://doi.org/10.1016/j.cej.2019.122102>

770 Kiziltaş, H., Tekin, T., Tekin, D., 2020. Preparation and characterization of recyclable  
771  $\text{Fe}_3\text{O}_4@\text{SiO}_2@\text{TiO}_2$  composite photocatalyst, and investigation of the photocatalytic  
772 activity. Chem. Eng. Commun. 0, 1–13.  
773 <https://doi.org/10.1080/00986445.2020.1743694>

774 Lee, G.-J., Lee, X.-Y., Lyu, C., Liu, N., Andandan, S., Wu, J.J., 2020. Sonochemical Synthesis  
775 of Copper-doped  $\text{BiVO}_4/\text{g-C}_3\text{N}_4$  Nanocomposite Materials for Photocatalytic  
776 Degradation of Bisphenol A under Simulated Sunlight Irradiation. Nanomaterials 10,  
777 498. <https://doi.org/10.3390/nano10030498>

778 Li, C., Mei, Y., Qi, G., Xu, W., Zhou, Y., Shen, Y., 2021. Degradation characteristics of four  
779 major pollutants in chemical pharmaceutical wastewater by Fenton process. J. Environ.  
780 Chem. Eng. 9, 104564. <https://doi.org/10.1016/j.jece.2020.104564>

781 Li, D., Yu, S.-H., Jiang, H.-L., 2018. From UV to Near-Infrared Light-Responsive Metal–  
782 Organic Framework Composites: Plasmon and Upconversion Enhanced Photocatalysis.  
783 Adv. Mater. 30, 1707377. <https://doi.org/10.1002/adma.201707377>

784 Li, Q., Wei, G., Yang, Y., Li, Z., Zhang, L., Shao, L., Lai, S., 2020. Insight into the enhanced  
785 catalytic activity of a red mud based  $\text{Fe}_2\text{O}_3/\text{Zn-Al}$  layered double hydroxide in the  
786 photo-Fenton reaction. Catal. Sci. Technol. 10, 7365–7377.  
787 <https://doi.org/10.1039/D0CY01539C>

788 Li, X.-K., Ji, W.-J., Zhao, J., Wang, S.-J., Au, C.-T., 2005a. Ammonia decomposition over Ru  
789 and Ni catalysts supported on fumed  $\text{SiO}_2$ , MCM-41, and SBA-15. J. Catal. 236, 181–  
790 189. <https://doi.org/10.1016/j.jcat.2005.09.030>

791 Liang, X., Zhong, Y., He, H., Yuan, P., Zhu, J., Zhu, S., Jiang, Z., 2012. The application of  
792 chromium substituted magnetite as heterogeneous Fenton catalyst for the degradation  
793 of aqueous cationic and anionic dyes. Chem. Eng. J. 191, 177–184.  
794 <https://doi.org/10.1016/j.cej.2012.03.001>

795 Liu, F., Yao, H., Sun, S., Tao, W., Wei, T., Sun, P., 2020. Photo-Fenton activation mechanism  
796 and antifouling performance of an FeOCl-coated ceramic membrane. *Chem. Eng. J.*  
797 402, 125477. <https://doi.org/10.1016/j.cej.2020.125477>

798 Liu, Ying, Liu, Yan, Shi, H., Wang, M., Cheng, S.H.-S., Bian, H., Kamruzzaman, M., Cao, L.,  
799 Chung, C.Y., Lu, Z., 2016. Cobalt-copper layered double hydroxide nanosheets as high  
800 performance bifunctional catalysts for rechargeable lithium-air batteries. *J. Alloys*  
801 *Compd.* 688, 380–387. <https://doi.org/10.1016/j.jallcom.2016.07.224>

802 Morshed, M.N., Pervez, M.N., Behary, N., Bouazizi, N., Guan, J., Nierstrasz, V.A., 2020.  
803 Statistical modeling and optimization of heterogeneous Fenton-like removal of organic  
804 pollutant using fibrous catalysts: a full factorial design. *Sci. Rep.* 10, 16133.  
805 <https://doi.org/10.1038/s41598-020-72401-z>

806 Nahim-Granados, S., Rivas-Ibáñez, G., Antonio Sánchez Pérez, J., Oller, I., Malato, S., Polo-  
807 López, M.I., 2020. Synthetic fresh-cut wastewater disinfection and decontamination by  
808 ozonation at pilot scale. *Water Res.* 170, 115304.  
809 <https://doi.org/10.1016/j.watres.2019.115304>

810 Nguyen, X.S., Pham, T.D., Vo, H.T., Ngo, K.D., 2021. Photocatalytic degradation of  
811 cephalexin by g-C<sub>3</sub>N<sub>4</sub>/Zn doped Fe<sub>3</sub>O<sub>4</sub> under visible light. *Environ. Technol.* 42, 1292–  
812 1301. <https://doi.org/10.1080/09593330.2019.1665110>

813 Ouyang, F., Li, H., Gong, Z., Pang, D., Qiu, L., Wang, Y., Dai, F., Cao, G., Bharti, B., 2020.  
814 Photocatalytic degradation of industrial acrylonitrile wastewater by F–S–Bi–TiO<sub>2</sub>  
815 catalyst of ultrafine nanoparticles dispersed with SiO<sub>2</sub> under natural sunlight. *Sci. Rep.*  
816 10, 12379. <https://doi.org/10.1038/s41598-020-69012-z>

817 Palanivel, B., Mudisoodum perumal, S. devi, Maiyalagan, T., Jayarman, V., Ayyappan, C.,  
818 Alagiri, M., 2019. Rational design of ZnFe<sub>2</sub>O<sub>4</sub>/g-C<sub>3</sub>N<sub>4</sub> nanocomposite for enhanced



819 photo-Fenton reaction and supercapacitor performance. *Appl. Surf. Sci.* 498, 143807.  
820 <https://doi.org/10.1016/j.apsusc.2019.143807>

821 Rad, T.S., Khataee, A., Rahim Pouran, S., 2018. Synergistic enhancement in photocatalytic  
822 performance of Ce (IV) and Cr (III) co-substituted magnetite nanoparticles loaded on  
823 reduced graphene oxide sheets. *J. Colloid Interface Sci.* 528, 248–262.  
824 <https://doi.org/10.1016/j.jcis.2018.05.087>

825 Rimoldi, L., Meroni, D., Falletta, E., Pifferi, V., Falciola, L., Cappelletti, G., Ardizzone, S.,  
826 2017a. Emerging pollutant mixture mineralization by TiO<sub>2</sub> photocatalysts. The role of  
827 the water medium. *Photochem. Photobiol. Sci.* 16, 60–66.  
828 <https://doi.org/10.1039/C6PP00214E>

829 Sahu, R.S., Shih, Y., Chen, W.-L., 2021. New insights of metal free 2D graphitic carbon nitride  
830 for photocatalytic degradation of bisphenol A. *J. Hazard. Mater.* 402, 123509.  
831 <https://doi.org/10.1016/j.jhazmat.2020.123509>

832 Sharma, K., Raizada, P., Hosseini-Bandegharaei, A., Thakur, P., Kumar, R., Thakur, V.K.,  
833 Nguyen, V.-H., Pardeep, S., 2020. Fabrication of efficient CuO / graphitic carbon nitride  
834 based heterogeneous photo-Fenton like catalyst for degradation of 2, 4 dimethyl phenol.  
835 *Process Saf. Environ. Prot.* 142, 63–75. <https://doi.org/10.1016/j.psep.2020.06.003>

836 Shyamala, R., Gomathi Devi, L., 2020. Reduced graphene oxide/SnO<sub>2</sub> nanocomposites for the  
837 photocatalytic degradation of rhodamine B: Preparation, characterization,  
838 photosensitization, vectorial charge transfer mechanism and identification of reaction  
839 intermediates. *Chem. Phys. Lett.* 748, 137385.  
840 <https://doi.org/10.1016/j.cplett.2020.137385>

841 Tao, Y., Monfort, O., Brigante, M., Zhang, H., Mailhot, G., 2021. Phenanthrene decomposition  
842 in soil washing effluents using UVB activation of hydrogen peroxide and

843 peroxydisulfate. Chemosphere 263, 127996.  
844 <https://doi.org/10.1016/j.chemosphere.2020.127996>

845 Wu, C.-K., Yin, M., O'Brien, S., Koberstein, J.T., 2006. Quantitative Analysis of Copper Oxide  
846 Nanoparticle Composition and Structure by X-ray Photoelectron Spectroscopy. Chem.  
847 Mater. 18, 6054–6058. <https://doi.org/10.1021/cm061596d>

848 Wu, Q., Yang, H., Kang, L., Gao, Z., Ren, F., 2020. Fe-based metal-organic frameworks as  
849 Fenton-like catalysts for highly efficient degradation of tetracycline hydrochloride over  
850 a wide pH range: Acceleration of Fe(II)/ Fe(III) cycle under visible light irradiation.  
851 Appl. Catal. B Environ. 263, 118282. <https://doi.org/10.1016/j.apcatb.2019.118282>

852 Wu, Y., Li, X., Zhao, H., Yao, F., Cao, J., Chen, Z., Ma, F., Wang, D., Yang, Q., 2022. 2D/2D  
853 FeNi-layered double hydroxide/bimetal-MOFs nanosheets for enhanced photo-Fenton  
854 degradation of antibiotics: Performance and synergetic degradation mechanism.  
855 Chemosphere 287, 132061. <https://doi.org/10.1016/j.chemosphere.2021.132061>

856 Wu, Y., Prulho, R., Brigante, M., Dong, W., Hanna, K., Mailhot, G., 2017. Activation of  
857 persulfate by Fe(III) species: Implications for 4-tert-butylphenol degradation. J. Hazard.  
858 Mater. 322, 380–386. <https://doi.org/10.1016/j.jhazmat.2016.10.013>

859 Xiao, J., Lai, J., Li, R., Fang, X., Zhang, D., Tsiakaras, P., Wang, Y., 2020. Enhanced  
860 Ultrasonic-Assisted Heterogeneous Fenton Degradation of Organic Pollutants over a  
861 New Copper Magnetite (Cu-Fe<sub>3</sub>O<sub>4</sub>/Cu/C) Nanohybrid Catalyst. Ind. Eng. Chem. Res.  
862 59, 12431–12440. <https://doi.org/10.1021/acs.iecr.0c01613>

863 Xiaoliang Fan, Cao, Q., Meng, F., Song, B., Bai, Z., Zhao, Y., Chen, D., Zhou, Y., Song, M.,  
864 2021. A Fenton-like system of biochar loading Fe–Al layered double hydroxides (FeAl-  
865 LDH@BC)/H<sub>2</sub>O<sub>2</sub> for phenol removal. Chemosphere 266, 128992.  
866 <https://doi.org/10.1016/j.chemosphere.2020.128992>

867 Yamashita, T., Hayes, P., 2008. Analysis of XPS spectra of Fe<sup>2+</sup> and Fe<sup>3+</sup> ions in oxide  
868 materials. Appl. Surf. Sci. 254, 2441–2449.  
869 <https://doi.org/10.1016/j.apsusc.2007.09.063>

870 Yang, J.E., Rossignol, E.D., Chang, D., Zaia, J., Forrester, I., Raja, K., Winbigler, H., Nicastro,  
871 D., Jackson, W.T., Bullitt, E., 2020. Complexity and ultrastructure of infectious  
872 extracellular vesicles from cells infected by non-enveloped virus. Sci. Rep. 10, 7939.  
873 <https://doi.org/10.1038/s41598-020-64531-1>

874 Yang, X., Chen, W., Huang, J., Zhou, Y., Zhu, Y., Li, C., 2015. Rapid degradation of methylene  
875 blue in a novel heterogeneous Fe<sub>3</sub>O<sub>4</sub>@rGO@TiO<sub>2</sub> -catalyzed photo-Fenton system. Sci.  
876 Rep. 5, 10632. <https://doi.org/10.1038/srep10632>

877 Yang, X., Ding, X., Zhou, L., Fan, H., Wang, X., Ferronato, C., Chovelon, J.-M., Xiu, G., 2020.  
878 New insights into clopyralid degradation by sulfate radical: Pyridine ring cleavage  
879 pathways. Water Res. 171, 115378. <https://doi.org/10.1016/j.watres.2019.115378>

880 Ye, Q., Xu, H., Wang, Q., Huo, X., Wang, Y., Huang, X., Zhou, G., Lu, J., Zhang, J., 2021.  
881 New insights into the mechanisms of tartaric acid enhancing homogeneous and  
882 heterogeneous copper-catalyzed Fenton-like systems. J. Hazard. Mater. 407, 124351.  
883 <https://doi.org/10.1016/j.jhazmat.2020.124351>

884 Zhang, H., Nengzi, L., Wang, Z., Zhang, X., Li, B., Cheng, X., 2020. Construction of  
885 Bi<sub>2</sub>O<sub>3</sub>/CuNiFe LDHs composite and its enhanced photocatalytic degradation of  
886 lomefloxacin with persulfate under simulated sunlight. J. Hazard. Mater. 383, 121236.  
887 <https://doi.org/10.1016/j.jhazmat.2019.121236>

888